*energies*

MDPI

*Article*

# Spatial and Temporal Variability of Ocean Thermal Energy Resource of the Pacific Islands

**Jessica Borges Posterari [1,*], Takuji Waseda [2], Takeshi Yasunaga [3] and Yasuyuki Ikegami [4]**

[1] Graduate Program in Sustainability Science, Graduate School of Frontier Sciences, The University of Tokyo, Kashiwa 277-8563, Japan
[2] Department of Ocean Technology, Policy and Environment, Graduate School of Frontier Sciences, The University of Tokyo, Kashiwa 277-8563, Japan; waseda@k.u-tokyo.ac.jp
[3] Faculty of Mechanical Engineering, Osaka Electro-Communication University, Neyagawa 572-8530, Japan; yasunaga@osakac.ac.jp
[4] Institute of Ocean Energy Saga, Saga University, Saga 840-8502, Japan; ikegami@cc.saga-u.ac.jp
* Correspondence: jessica.posterari@s.k.u-tokyo.ac.jp; Tel.: +81-08089166008

**Abstract:** A lack of natural resources drives the oil dependency in Pacific Island Countries and Territories (PICTs), hampering energy security and imposing high electricity tariffs in the region. Nevertheless, the Western Equatorial Pacific is known for its large Sea Surface Temperature (SST) and deep-sea water (DSW) temperature difference favorable for harvesting thermal energy. In this study, we selected 18 PICTs in the western Equatorial Pacific to estimate Annual Energy Production (AEP) for a 1 MW class Ocean Thermal Energy Conversion (OTEC) plant. We combined the DSW temperature from the mean in situ Argo profiles and 1 km resolution satellite SST data to estimate the thermal energy resource resolving the fine features of the island coastline. Furthermore, the twenty-year-long SST dataset was used to analyze the SST variability. The analysis showed that Equatorial islands and Southern islands have the highest inter-annual variability due to El Nino Southern Oscillation (ENSO). The power density varied from 0.26 to 0.32 W/m$^2$ among the islands, with the lowest values found for the southernmost islands near the South Equatorial Countercurrent. Islands within the South Equatorial Current, Equatorial Undercurrent, and North Equatorial Countercurrent showed the highest values for both power density and gross power. Considering a 1 MW class OTEC plant, Annual Energy Production (AEP) in 2022 varied from 7 GWh to 8 GWh, with relatively low variability among islands near the Equator and in low latitudes. Considering the three variables, AEP, SST variability, and distance from the shore, Nauru is a potential candidate for OTEC, with a net power of 1.14 MW within 1 km from the shore.

**Keywords:** ocean thermal energy; Pacific islands; Pacific Ocean; high-resolution sea surface temperature; ocean thermal resource variability



**Citation:** Borges Posterari, J.; Waseda, T.; Yasunaga, T.; Ikegami, Y. Spatial and Temporal Variability of Ocean Thermal Energy Resource of the Pacific Islands. *Energies* **2024**, *17*, 2766. https://doi.org/10.3390/en17112766

Academic Editors: Andrea Frazzica, Eugen Rusu, Kostas Belibassakis and George Lavidas

Received: 4 February 2024
Revised: 1 May 2024
Accepted: 2 May 2024
Published: 5 June 2024



## 1. Introduction

Pacific Island Countries and Territories (PICTs) are small islands in the Pacific Ocean, but their territorial sea and Exclusive Economic Zone occupy 40% of the ocean's surface. A reduction in the region's dependency on diesel meets their goal of sustainable development. Ocean thermal resources are abundant and can be further explored as a source of energy through Ocean Thermal Energy Conversion (OTEC). OTEC technology uses the temperature difference between the ocean surface and deep-sea water to generate electricity, with a minimum temperature difference threshold of 20 °C within a 1000 m depth, which benefits steep bathymetry regions with high SST. Even though offshore platforms have been conceptualized, land-based OTEC plants with DSW pipelines are still the main type of installation.

To study the feasibility of OTEC in the PICTs, ocean energy resources need to be estimated on a local scale. High-resolution, long-term oceanographic data become necessary.

The challenges of representing the islands of the PICTS arise not only from their small land sizes but also from the unique climate features of the region. The Tropical Pacific Ocean is a complex system with several dominant surface currents (North/South Equatorial Current, North/South Equatorial Countercurrent) and subsurface currents (Equatorial Under Current). The Sea Surface Temperature (SST) has a large zonal contrast along the Equator between the Western and Eastern Equatorial Pacific driven by Walker circulation [1], creating a warm pool in the West and a cold tongue in the East.

Figure 1 shows the areas where the temperature difference between the sea surface and 1000 m depth is higher than 18 °C. The warm pool in the Western Equatorial Pacific is particularly relevant for OTEC, with temperature differences ranging from 24 to 26 °C. However, several islands are in transition zones. Particularly, the Southern Islands are close to the sub-tropics, and therefore, the seasonal change is relatively large. For these reasons, the ocean thermal energy potential of each island may vary. Moreover, the Tropical Pacific Ocean is affected by El-Nino/Southern Oscillation (ENSO), and the inter-annual variability of the SST of the PICTs has not yet been analyzed on a local scale.

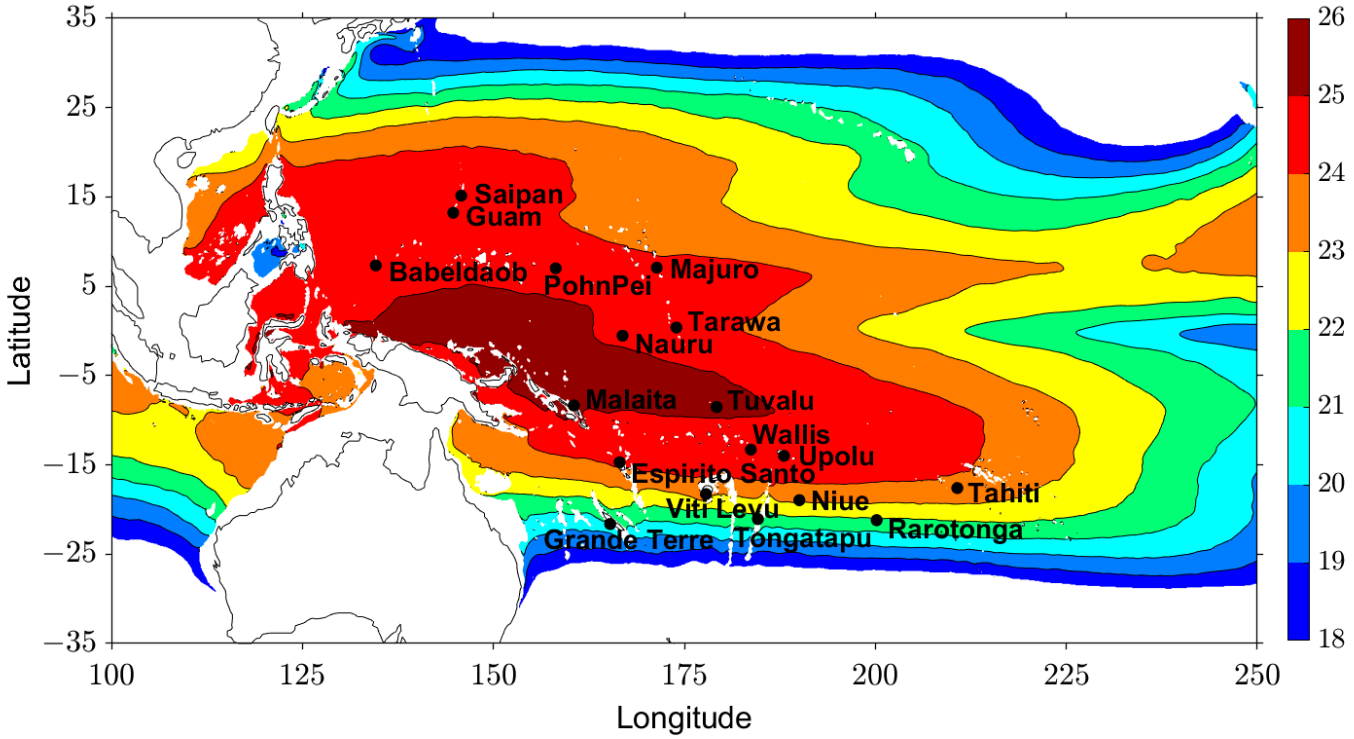


**Figure 1.** Temperature difference between surface and 1000 m depth using the HYCOM GOFS 3.1 [2] climatology data from 1994 to 2015. The map only shows the areas where the temperature difference is higher than 18 °C. Black circles represent the 18 islands considered for this study.

There have been studies in the past assessing the potential for OTEC in the PICTs, which have also included a comparison between islands. In 2001, the SOPAC (South Pacific Applied Geoscience Commission) released a report detailing unit cost for OTEC compared to conventional energy sources, as well as temperature difference data for eight PICTs [3]. In 2010, Vega [4] published a study on Ocean Thermal Conversion, estimating global ocean thermal resources using temperature data from WOA05 [5]. His study identified 15 PICTs with adequate resources ($\Delta T > 20$ °C). Kim et al. [6] reviewed the advantages of OTEC, available technologies, economics, and its applications to Pacific islands based on available literature. Furthermore, Petterson and Kim [7] focused their study on Kiribati, discussing a 1 MW OTEC plant in South Tarawa.

Global OTEC resources have also been reviewed and explained in the International Renewable Energy Agency (IRENA) [8] and Asian Development Bank (ADB) [9] reports, including potential candidates for OTEC, technology brief, and cost analysis. The global

resources for OTEC have been estimated by Rajagopalan & Nihous [10] using WOA05 data with 1° horizontal grid resolution, showing that, at 1000 m depth, it is possible to find a 24 to 26 °C temperature difference in the surface water in the Western Equatorial Pacific. Even though the currently available datasets for ocean temperature can provide information on ocean thermal power on a global scale, including the PICTs, the data have limitations related to their coarse resolution. Perhaps a global map is only relevant at the very early stage of development, where a potential site is selected among different oceans.

There are several available approaches to generating high-resolution temperature data, which can vary from ocean models to simplified methods based on observational data. Several operational global ocean models were developed under the Global Ocean Data Assimilation Experiment (GODAE) initiative, and their products are available for various applications [11]. Aiming to resolve ocean mesoscale, their resolutions are typically in the order of 1/10 degree, and higher-resolution products are still being developed. These products rely on the altimeter-based sea surface height, which became a routine observation in 1994. Therefore, the typical time range of these products is nearly 30 years by now. In Figure 1, we utilize the 21-year Global Ocean Forecasting System (GOFS) 3.1 output, which has both analysis and reanalysis data available on a 1/12° horizontal grid HYCOM model [2]. The progress on operational ocean models over the past three decades is significant, but in terms of the PICTs, the model resolution is still not high enough, as PICTs include some of the world's smallest island nations, which are misrepresented or omitted in global products.

A natural extension of the GODAE products is to develop a regional high-resolution ocean model nested within the global model. One example of such a regional model was developed around Hawaii as part of the Pacific Islands Integrated Ocean Observing System [12]. This is undoubtedly the last thing we should do, but in the feasibility study stage of the development, which is the aim of this study, it is not a suitable choice as all the 18 islands are geographically isolated, which means that 18 regional models need to be developed. Therefore, we need an alternative approach that enables us to conduct a quick assessment and select an island for developing a regional model.

Doorga et al. [13] proposed an algorithm to estimate power generated by OTEC in Mauritius Island by processing 1 km resolution satellite data combined with bathymetry data, Argo temperature profile data, and AVISO altimetry data. They successfully estimated the net power generated from an OTEC power plant at a resolution of 1 km while resolving the four monsoonal seasons. This study, therefore, adapted the method proposed by Doorga et al. to our case studies and focused on analyzing ocean temperature data for all 18 islands using a combination of a 1 km resolution satellite-derived SST data and in situ temperature measurements from Argo. Making use of the 20 years of data from the Multi-scale Ultra-high Resolution (MUR) Sea Surface Temperature (SST) Analyses (hereafter MURSST) [14], as well as 20 years of Argo temperature profiles, we were able to estimate the climatology, seasonal climatology, and monthly climatology of the temperature profiles for each island.

Figure 2 summarizes how these datasets are utilized in this study. Spatio-temporal mean temperature profiles were obtained for the 18 islands, and based on their characteristics, the islands were grouped into five categories. The SST climatology from the MURSST dataset was used to assess the climate variations of the 18 islands, with a particular focus on the impact of ENSO events. Finally, the two datasets were combined to assess the OTEC resources of the 18 islands, with the mean Argo Profiles providing DSW temperature and the MURSST providing a 1 km gridded SST.

The objectives of the present study are to (1) analyze the SST climatology and variability for 18 islands and obtain the local temperature profiles, as well as (2) combine the in situ data and high-resolution SST data to map OTEC resources and evaluate the feasibility of OTEC for the 18 islands. The final goal is to be able to better understand the distribution of ocean thermal energy in the Pacific Ocean.

Section 2 describes how the 18 islands were selected from the 22 PICTs for further analysis. Oceanographic and climatological descriptions of the ocean area, including the 18 islands, are presented in Section 3. Ocean thermal energy resources are estimated in Section 4. A discussion follows.

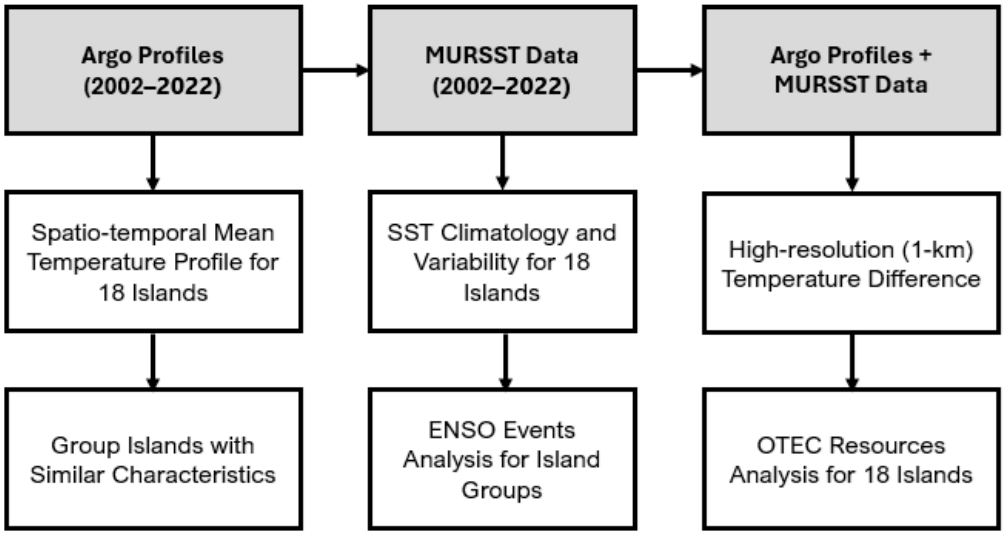


**Figure 2.** Flow chart demonstrating how each dataset was used, leading to the outputs necessary for ocean thermal energy assessment, combining Argo profiles and MURSST data.

## 2. Pacific Island Countries and Territories

A total of 22 classified Pacific Island Countries and Territories were considered for analysis. The selection process prioritized the most populated island of each country and territory as the goal is to supply energy to a high-demand area. Among the 22 analyzed countries and territories, 18 islands were selected using demographic data as the main variable. Table 1 contains each island selected for this study, as well as the coordinates of the domain for data extraction purposes. The rectangular domain was chosen as approximately 30 km from the southernmost, northernmost, easternmost, and westernmost points of each island. Global OTEC studies have used a 100 km distance for analysis in the past [15]; however, due to the land size limitations and cost constraints for OTEC in the Pacific, a shorter distance of 30 km was defined here. The domain had to be large enough to include a higher number of in situ measurements within the domain, as the measurements are often limited in spatial availability while still being kept appropriate to represent the local area using the mean temperature profile.

Based on the climatology of SST, local bathymetry data, and horizontal distance to the shore, one site was selected for each island for further OTEC analysis and comparison purposes. Analysis was carried out using ArcGIS Pro; first, a mask for the land surface was created using the MURSST mask; second, a mask for the ocean area where bathymetry was between 0 m and 700 m depths was created using GEBCO data [16]; lastly, sites were selected based on the minimum distance between land and DSW extraction (700 m depth), prioritizing areas with higher SST. Table 2 details the site coordinates, distance to the shore, and closest district for all 18 islands.

**Table 1.** Islands selected for this study and their respective domains, ordered from the highest-population to the lowest-population island.

| Number | Island | Country | North | South | West | East |
|---|---|---|---|---|---|---|
| 1 | Viti Levu | Fiji | 16.51 S | 19.00 S | 176.38 E | 179.55 E |
| 2 | Malaita | Solomon Islands | 8.08 S | 9.83 S | 160.11 E | 162.08 E |
| 3 | Espirito Santo | Vanuatu | 16.97 S | 18.37 S | 167.58 E | 169.27 E |
| 4 | Grande Terre | New Caledonia | 18.53 S | 23.73 S | 162.35 E | 168.77 E |
| 5 | Tahiti | French Polynesia | 17.30 S | 18.05 S | 149.84 W | 148.91 W |
| 6 | Upolu | Samoa | 14.36 S | 13.48 S | 172.38 W | 171.06 W |
| 7 | Guam | Guam | 12.94 N | 13.97 N | 144.31 E | 145.24 E |
| 8 | Tarawa | Kiribati | 1.03 N | 1.93 N | 172.59 E | 173.47 E |
| 9 | Pohnpei | Micronesia | 6.46 N | 7.38 N | 157.76 E | 158.66 E |
| 10 | Tongatapu | Tonga | 21.56 S | 20.77 S | 175.68 W | 174.71 W |
| 11 | Saipan | Northern Mariana | 14.81 N | 15.60 N | 145.39 E | 146.15 E |
| 12 | Majuro | Marshall Islands | 6.75 N | 7.52 N | 170.71 E | 171.71 E |
| 13 | Babeldaob | Palau | 6.65 N | 8.32 N | 133.88 E | 134.97 E |
| 14 | Rarotonga | Cook Islands | 21.57 S | 20.91 S | 160.15 W | 159.40 W |
| 15 | Wallis | Wallis and Futuna | 13.68 S | 12.87 S | 176.57 W | 175.83 W |
| 16 | Tuvalu | Tuvalu | 8.94 S | 8.13 S | 178.73 E | 179.50 E |
| 17 | Nauru | Nauru | 0.84 S | 0.21 S | 166.61 E | 167.26 E |
| 18 | Niue | Niue | 19.44 S | 18.64 S | 170.28 W | 169.46 W |

**Table 2.** Location details for selected sites for all 18 islands.

| | Offshore Coordinates | | Onshore Coordinates and Information | | | |
|---|---|---|---|---|---|---|
| **Island** | **Latitude** | **Longitude** | **Latitude** | **Longitude** | **Distance to DSW (m)** | **Closest District** |
| Tuvalu | 8.53 S | 179.22 E | 8.53 S | 179.21 E | 319 | Fongafale |
| Nauru | 0.54 S | 166.91 E | 0.53 S | 166.91 E | 384 | Boe |
| Tarawa | 0.38 N | 173.95 E | 0.38 N | 173.94 E | 444 | Bonriki |
| Rarotonga | 21.19 S | 159.83 W | 21.20 S | 159.82 W | 632 | Arorangi |
| Upolu | 13.99 S | 171.96 W | 13.98 S | 171.96 W | 856 | Vavau |
| Niue | 18.95 S | 169.95 W | 18.95 S | 169.88 W | 867 | Vaiea |
| Saipan | 15.14 N | 145.79 E | 15.15 N | 145.79 E | 1030 | Naftan |
| Espirito Santo | 14.71 S | 166.52 E | 14.71 S | 166.53 E | 1413 | Petani |
| Majuro | 7.08 N | 171.39 E | 7.09 N | 171.38 E | 1455 | Ajeltake |
| Babeldaob | 7.33 N | 134.60 E | 7.34 N | 134.59 E | 1588 | Airai |
| Malaita | 8.35 S | 160.53 E | 8.35 S | 160.55 E | 1693 | Aenalite |
| Tahiti | 17.60 S | 149.27 W | 17.60 S | 149.29 W | 1915 | Puna'auia |
| Tongatapu | 21.07 S | 175.37 W | 21.09 S | 175.35 W | 1934 | Ha'atafu |
| Guam | 13.23 N | 144.74 E | 13.24 N | 144.73 E | 1958 | Asan |
| Viti Levu | 18.27 S | 177.82 E | 18.25 S | 177.83 E | 2755 | Komave |
| Grande Terre | 21.62 S | 165.29 E | 21.58 S | 165.30 E | 3880 | Nessadiou |
| PohnPei | 7.01 N | 158.16 E | 6.98 N | 158.17 E | 4169 | Palikir |
| Wallis | 13.29 S | 176.30 W | 13.29 S | 176.25 W | 4706 | Vaimalau |

## 3. Oceanographic and Climatological Characteristics of the PICTs

### *3.1. Vertical Temperature Profile*

Argo profiling data were averaged for all the cycles in the analysis domain (Table 1) from 2002 to 2022. The depth range was from 0 m to 2000 m every 20 m. Figure 3 left shows an example of the spatial distribution of the 30 Argo cycles for the island of Nauru, in which the Southwest quadrant has the largest number of profiles. The number of floats

and number of Argo profiling cycles vary among islands and are summarized in Table A1 (Appendix A). The temperature data were averaged, where $\overline{T}(z)$ is the mean temperature and $s(z)$ is the standard deviation, and $n$ is the total number of cycles.

$$\overline{T}(z) = \frac{1}{n}\sum_{i=1}^{n} T_i(z) \quad (1)$$

$$s(z) = \sqrt{\frac{\sum_{i=1}^{n}\left(T_i(z) - \overline{T}(z)\right)^2}{(n-1)}} \quad (2)$$

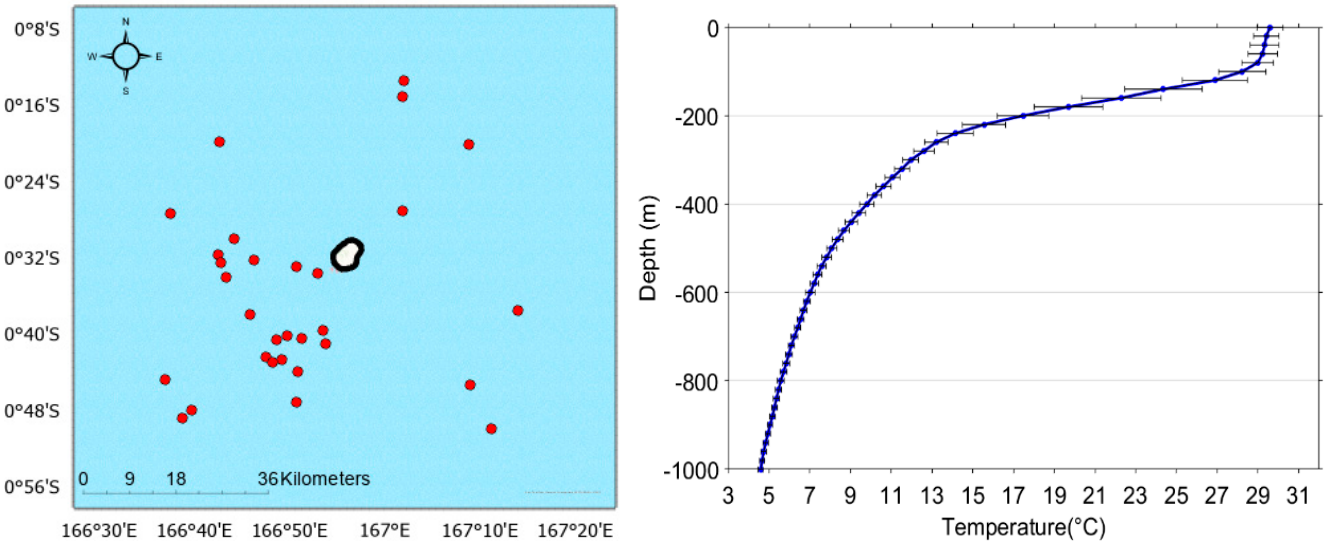


**Figure 3.** (**Left**) Coordinates of the Argo profiles for the Nauru island analysis, including 30 cycles. Red circle represents the location of each profile, black contour represents the island. (**Right**) Averaged Temperature Profile for the island of Nauru with standard deviation bars for each depth, using Argo climatology data from 2002 to 2022.

Figure 3 right shows an example of the mean temperature profile from a 0 m to 1000 m depth with the standard deviation as an error bar. Using 20 years of Argo profiling data, the highest standard deviation was found to be within the first 200 m. As depth increases, the standard deviation decreases, reaching values in the range of 0.1–0.2 °C between 500 and 1000 m. Due to the low temperature variation at deeper depths, the temperature was assumed to be homogeneous in the domain at depths between 500 m and 1000 m.

### *3.2. Classification of the Islands*

We classified the 18 islands into 5 groups using the Argo temperature profiles. The profiles bear typical tropical ocean characteristics where the mean temperature rapidly drops in the permanent thermocline, below the shallow warm mixed layer (Figure 4). The SST of the islands varies between 24 and 28 °C, but the DSW temperature seems to be the same. The profiles in Figure 4 are colored to identify their groups for visual aid. The classification is based not only on the temperature profiles and will be augmented by the island locations and the underlying ocean current field (Table 3). For each group, the temperature profiles are averaged, and the mean profiles are shown in Figure 5 left. The most notable difference among the islands is the thermocline structure. For example, the depth where the temperature drops to around 10 °C varies between 200 m and 500 m. It then seems plausible to classify the islands by the transition depth from the thermocline to the DSW. We call this depth the thermocline depth.

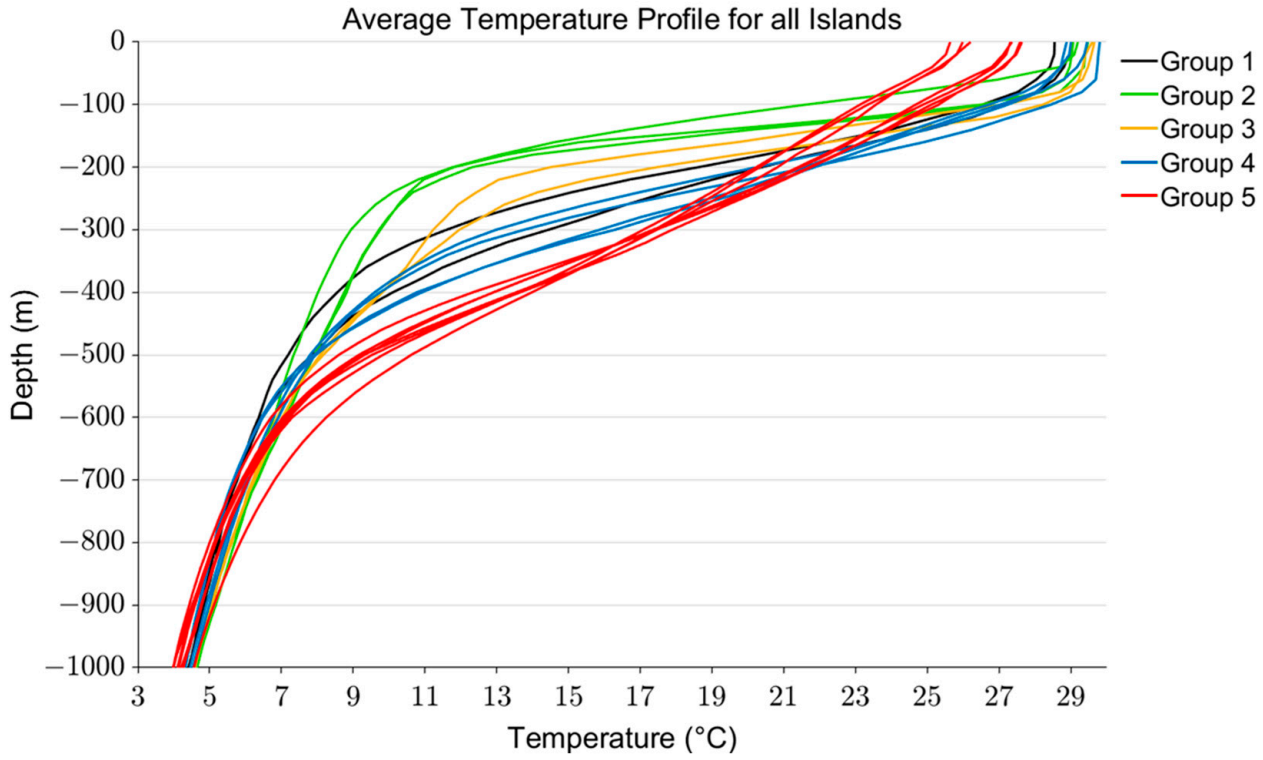


**Figure 4.** Average temperature profiles for all 18 islands based on Argo measurements from 2002 to 2022 in the analysis domain (Table 1). Black represents Group 1, green represents Group 2, yellow represents Group 3, blue represents Group 4, and red represents Group 5.

**Table 3.** Summary of the five island groups, including information for currents, temperature, and final remarks.

| Group | Current | T0 m | T200 m | T400 m | T600 m | T800 m | Remarks |
|---|---|---|---|---|---|---|---|
| 1. | North Equatorial Current | 28.51 | 19.51 | 9.33 | 6.42 | 5.24 | Northern hemisphere with seasonal Variability |
| 2. | North Equatorial Counter Current | 29.39 | 11.97 | 8.53 | 6.65 | 5.3 | The rapid decrease in temperature at 200 m |
| 3. | Equatorial Under Current | 29.48 | 15.98 | 9.81 | 6.95 | 5.6 | Affected by ENSO and interannual variability |
| 4. | South Equatorial Counter Current | 29.38 | 21.37 | 10.26 | 6.65 | 5.3 | Southern hemisphere with seasonal variability |
| 5. | South Equatorial Current | 26.70 | 21.10 | 13.28 | 7.25 | 5.28 | Lowest SST, affected by ENSO and interannual variability |

Temperature gradients from the average temperature profiles of each group are shown in Figure 5 right. The density gradient increases in the thermocline up to 1 to 2.5 °C/m and decreases gradually with depth. We define the thermocline depth where the density gradient in the thermocline reduces to 0.4 °C/m. We found that temperature decreases rapidly in the thermocline for groups 2 and 3, with shallow thermocline depths (Group 2 at 280 m and Group 3 at 340 m). Group 5 had the deepest thermocline depth at 580 m while having the lowest rate of temperature change up to a 380 m depth, starting to bear midlatitude characteristics. Groups 1 and 4 show similar values of thermocline depth, 440 m and 480 m, respectively, but they are located in opposite hemispheres. If we consider the depth for a temperature difference of 20 °C for OTEC purposes (dots in Figure 5 left), we can see that Group 2 has the lowest access at 320 m, followed by Groups 3, 1, and 4. Regarding temperature at the thermocline depth, Group 3 had the highest, at 11.2 °C, followed by Group 2, at 9.9 °C.

We now classify the islands into 5 groups and show how access to deep-sea water changes with latitude (Figure 6). We found that, overall, the thermocline becomes shallower toward the Equator and deepens toward the tropics. Groups 2 and 3 provide the easiest access to DSW at lower thermocline depths, which are less than 350 m, while Group 5 had the deepest thermocline depth, varying between 550 and 600 m. Temperature profiles were split for each group in Figure 7 for a better presentation of temperature variation with depth for each island. It turns out that this classification is consistent with the background ocean current field, as shown in Table 3. We will now discuss the oceanographic justification of the classification.

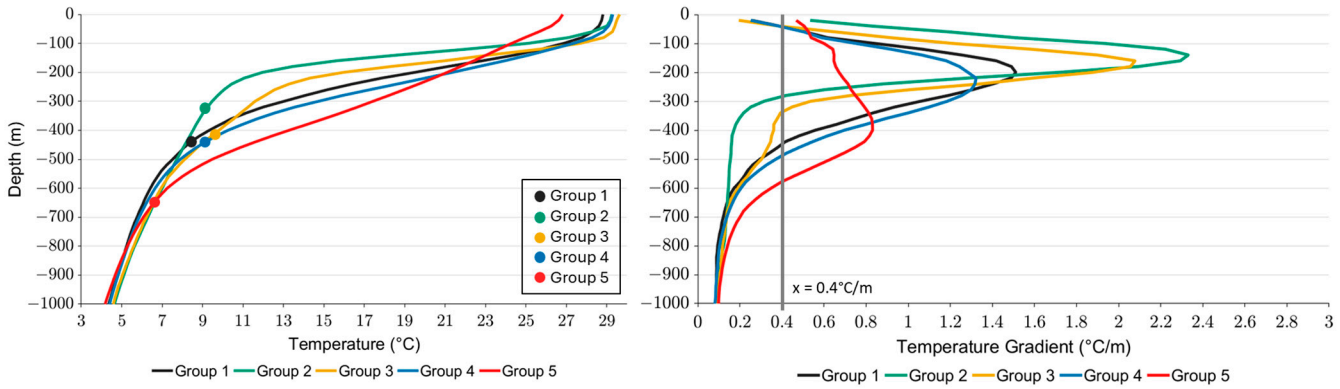


**Figure 5.** Average temperature profiles for each group, showing the depth where temperature difference reaches 20 °C (**left**) and average temperature gradient for each group (**right**) based on Argo measurements from 2002 to 2022 and domain coordinates from Table 1.

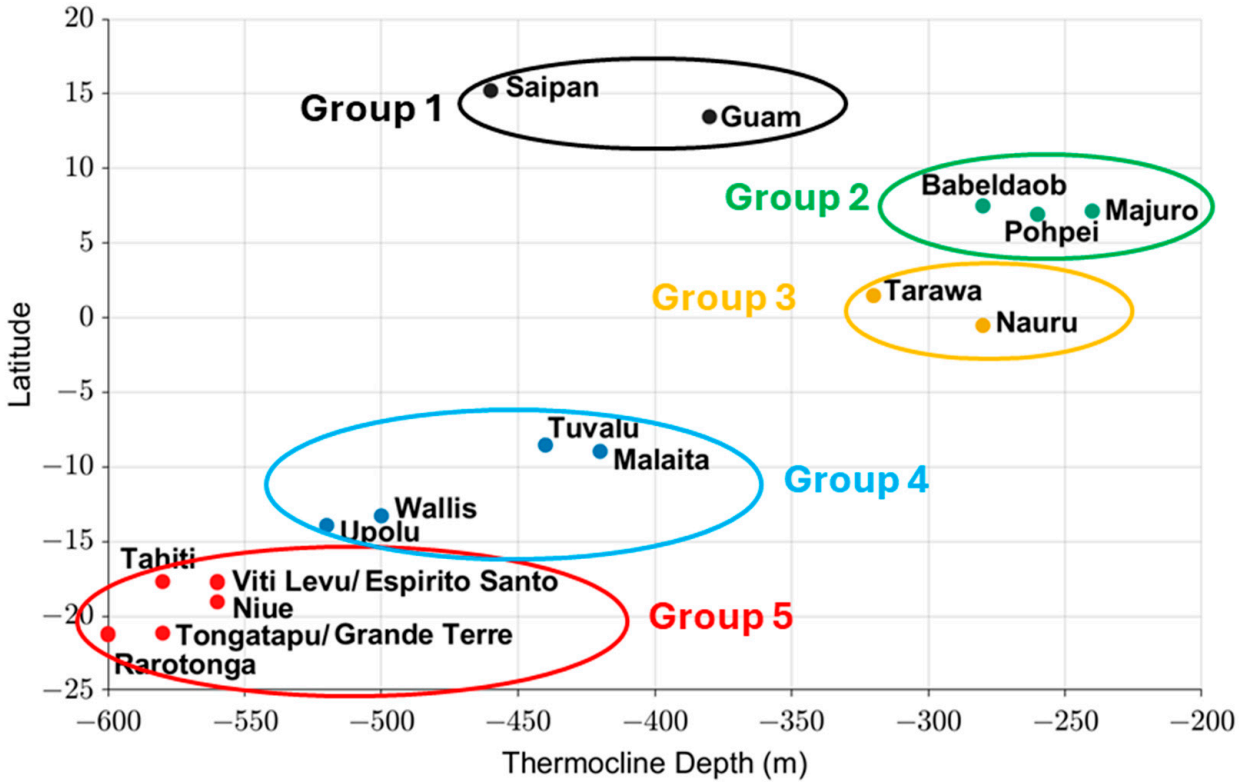


**Figure 6.** DSW depth (m) versus latitude for all 18 islands based on Argo measurements from 2002 to 2022 and domain coordinates from Table 1. Black represents Group 1, green represents Group 2, yellow represents Group 3, blue represents Group 4, and red represents Group 5.

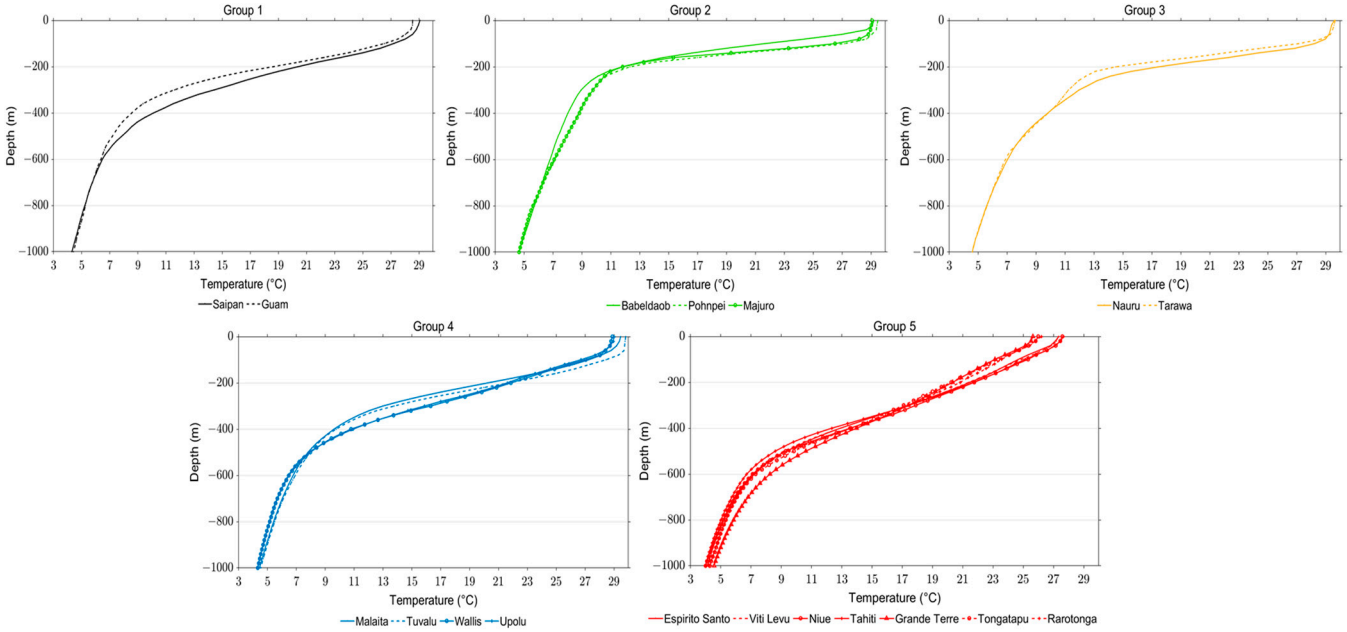


**Figure 7.** Average temperature versus depth for Group 1, Group 2, Group 3, Group 4, and Group 5 based on Argo measurements from 2002 to 2022 and domain coordinates from Table 1.

In the Tropical Pacific, from the north to the south, the dominant surface currents are the westward North Equatorial Current (NEC) and the eastward North Equatorial Counter Current (NECC) in the northern hemisphere. In the southern hemisphere, the current fields are less well-defined because of the monsoon influence. The westward South Equatorial Current (SEC) occupies a broader latitudinal range from 20° S to near the Equator, and there is an opposing current flowing eastward called the South Equatorial Counter Current (SECC) at latitudes north of 5° S (Figure 8 top). At the Equator, the Equatorial Under Current (EUC) flows eastward at a depth of 150 m (Figure 8 bottom). These dominant current fields are well represented in HYCOM GOFS 3.1. The majority of the islands are located within the western Pacific "warm pool", where the SST is higher than 28 degrees (Figure 9). The SST of these islands is higher than that of regions near the Tropic of Cancer, where the existing OTEC plants in Kume Island and Hawaii Island are located. The SST of the island regions near the Tropic of Capricorn are much lower, ranging from around 25 to 27 degrees.

Based on this oceanographic information, the 18 islands are classified into 5 groups (Table 3). The group numbers are given as 1 to 5 from north to south, and acronyms of the representative current fields are annotated in Figure 8 top as a guide.

**[Group 1]** ***Guam*** and ***Saipan*** are under the influence of the NEC and have a shallow mixed layer depth. Temperature decreases from the surface until approximately 600 m.
**[Group 2]** The islands of ***Babeldaob***, ***Majuro***, and ***Pohnpei*** are in regions where the NECC flows. Although having varied mixed layer depths, their temperature profiles show a similar pattern of a high decrease in temperature until 200 m, followed by a slow decrease in temperature up to 1000 m. The large drop in temperature in the upper 200 m is because of the shallow NECC.
**[Group 3]** ***Nauru*** and ***Tarawa*** islands are located where the EUC flows. The main difference from the other groups is the higher temperatures until 600 m and the higher surface temperatures. The current speed reverses from the surface to the subsurface, where the EUC flows at a depth of around 150 m to 200 m, and the velocity reaches up to 1.2 m/s, increasing eastward.
**[Group 4]** ***Malaita***, ***Tuvalu***, ***Upolu***, and ***Wallis*** are in the upstream of the SECC. The temperature profiles resemble Group 1 despite being affected by completely different current fields. It is characterized by a shallow mixed layer depth and a gradual decrease

in temperature from the surface until approximately 600 m. The 200 m temperature is the highest among the five groups.

**[Group 5]** ***Grande Terre***, ***Espirito Santo***, ***Tahiti***, ***Viti Levu***, ***Niue***, ***Rarotonga***, and ***Tongatapu*** are the southernmost islands and are located in the SEC. They are characterized by a shallow mixed layer depth and a gradual decrease in temperature from the surface until approximately 600 m. The 400 m depth temperature is the warmest among the five groups.

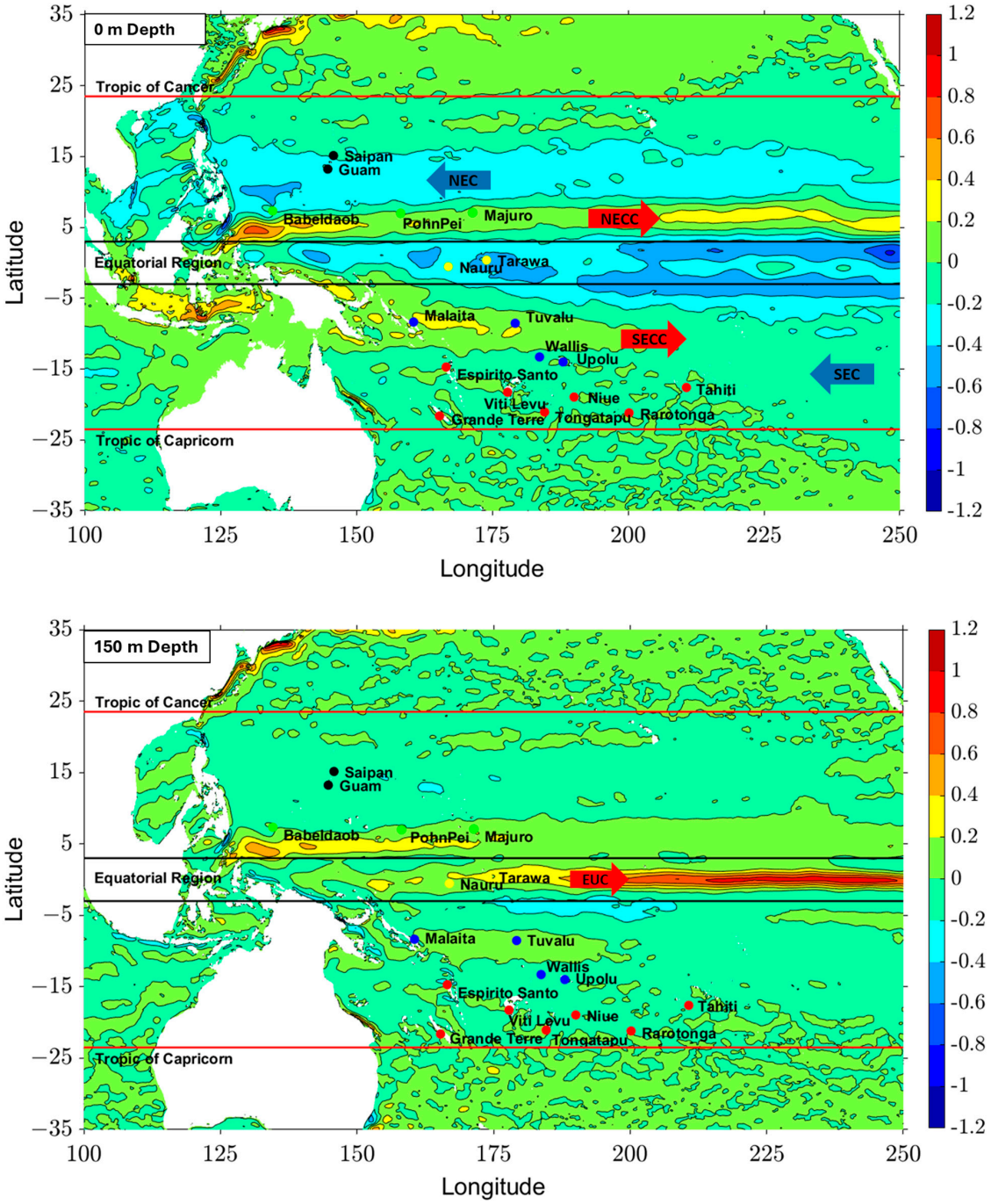


**Figure 8.** Map with climatology of eastward velocity (m/s) at 0 m depth (**top**) and 150 m depth (**bottom**) using HYCOM GOFS 3.1 reanalysis data (1994–2015), including Equatorial region (between −3° N and 3° S), Tropic of Cancer, and Tropic of Capricorn). Black circles represent Group 1, green circles represent Group 2, yellow circles represent Group 3, blue circles represent Group 4, and red circles represent Group 5. Velocity varies from −1.2 to 1.2 m/s.

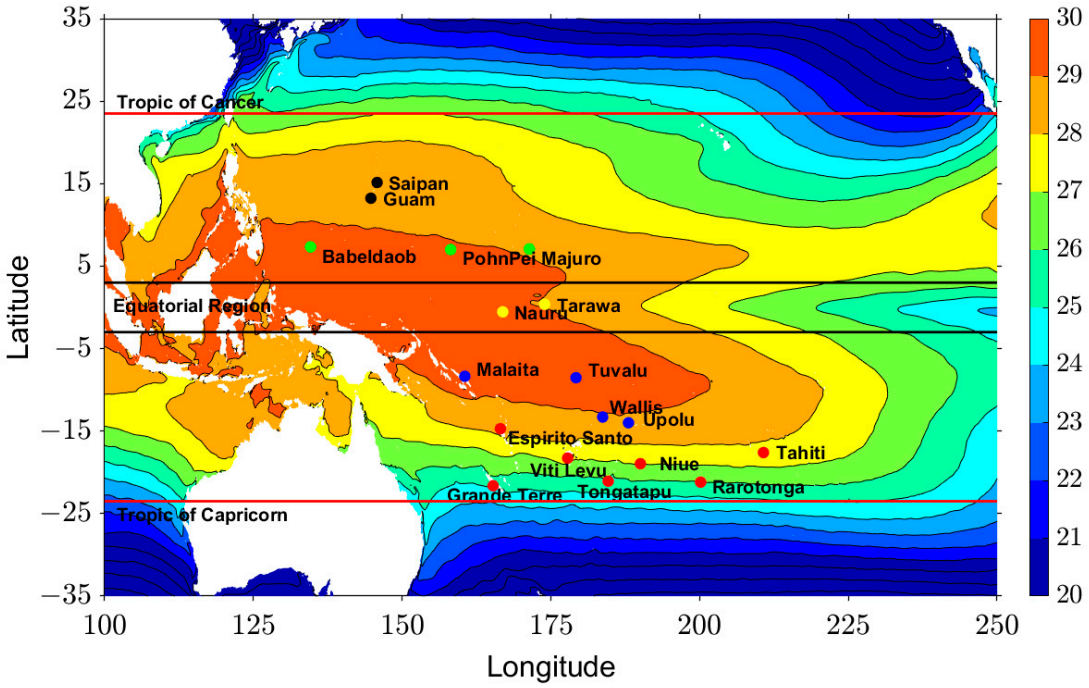


**Figure 9.** The SST (°C) climatology from HYCOM GOFS 3.1 reanalysis data (1994–2015), including the Equatorial region (between −3° N and 3° S), Tropic of Cancer, and Tropic of Capricorn. Black circles represent Group 1, green circles represent Group 2, yellow circles represent Group 3, blue circles represent Group 4, and red circles represent Group 5. Temperature varies from 20 to 30 °C.

### *3.3. SST Climatology and Variability*

The Sea Surface Temperature (SST) is the key variable for OTEC analysis. For clear, open ocean waters, 55% of the incoming solar energy is absorbed in the first meter of the water column, while more than 90% is absorbed in the first 15 m [17]. Thus, the vast majority of solar incidence is limited to the surface layer, where solar energy is converted into heat. Due to the seasonal changes and varying geographical distribution of SST, we analyzed the SST climatology (average of 20 years) and seasonal SST climatology (20-year average of each season). Figure 10 shows the SST climatology for the Pacific domain, including all 18 islands, while Figure 11 shows the seasonal SST climatology; the same color range was applied for all figures.

Inside the warm pool area, SST remains high throughout the seasons, showing small seasonal variability. The Southeastern area has high temperatures during the first (December–February) and second seasons (March–May); nevertheless, if we investigate the climatology, the Southeastern areas have lower temperatures on average. Northwestern areas maintain high temperatures throughout the seasons, with peak SST happening during the third season, which represents summer in the northern hemisphere. The eastern area located near the Equator line has low SST values for all seasons, as well as for the climatology data, rendering it less suitable for OTEC development. Overall, the largest seasonal variations are found within the southern tropics, while the least variability is found in the Western Equatorial Pacific region, where the warm pool is located.

SST climatology data were compared to the climatology data obtained from Argo measurements for all 18 islands, as shown in Figure 12. The difference between SST climatology from MURSST and Argo SST remained less than 1 °C for all islands, which is approximately a 3% difference. The largest difference between MURSST and Argo SST was found to be at Saipan (0.924 °C) and Espirito Santo (0.833 °C), which are located in the Northern and Southern parts of the Equatorial Pacific, respectively. In other islands, the difference between MURSST and Argo SST was less than 1%. Therefore, assuming that Argo is providing reliable measurements, we conclude that MURSST data are suitable for further analysis.

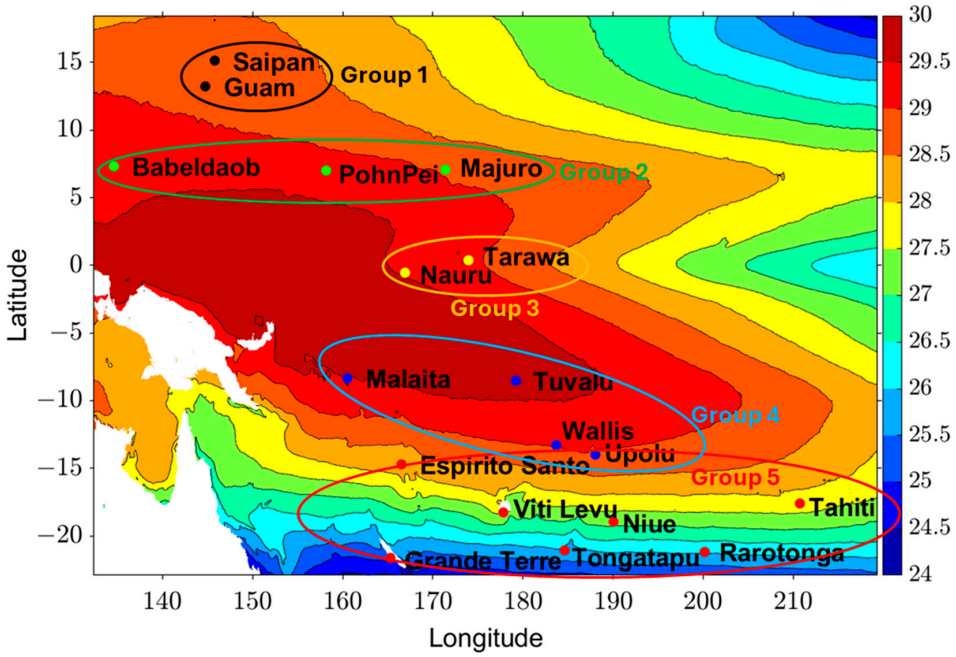


**Figure 10.** SST climatology data for the Pacific domain using MURSST data from 2002 to 2022. Black circles represent Group 1, green circles represent Group 2, yellow circles represent Group 3, blue circles represent Group 4, and red circles represent Group 5.

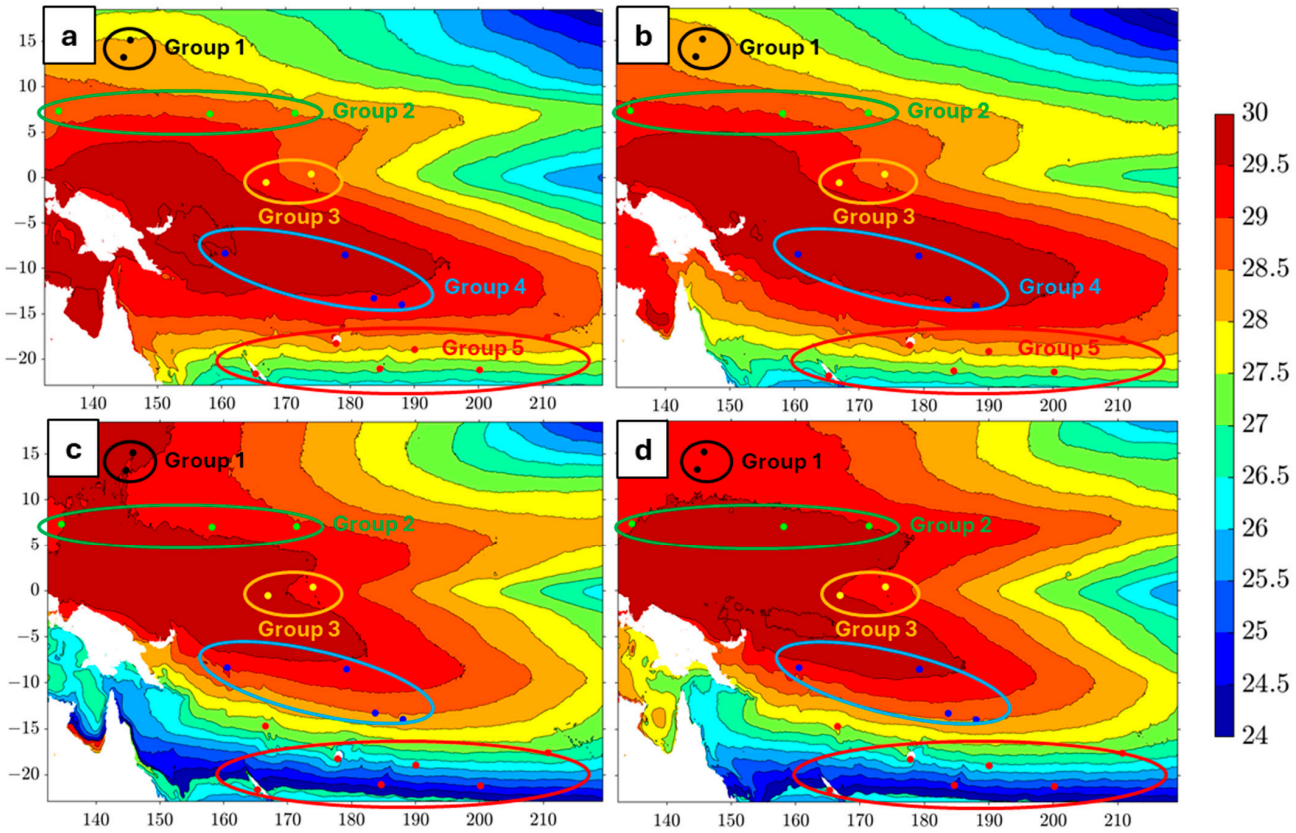


**Figure 11.** SST seasonal climatology data for the Pacific domain using MURSST data from 2002 to 2022. (**a**) is 1st season (December–February), (**b**) is 2nd season (March–May), (**c**) is 3rd season (June–August), and (**d**) is 4th season (September–November). The temperature varies between 24 and 30 °C for all four plots.

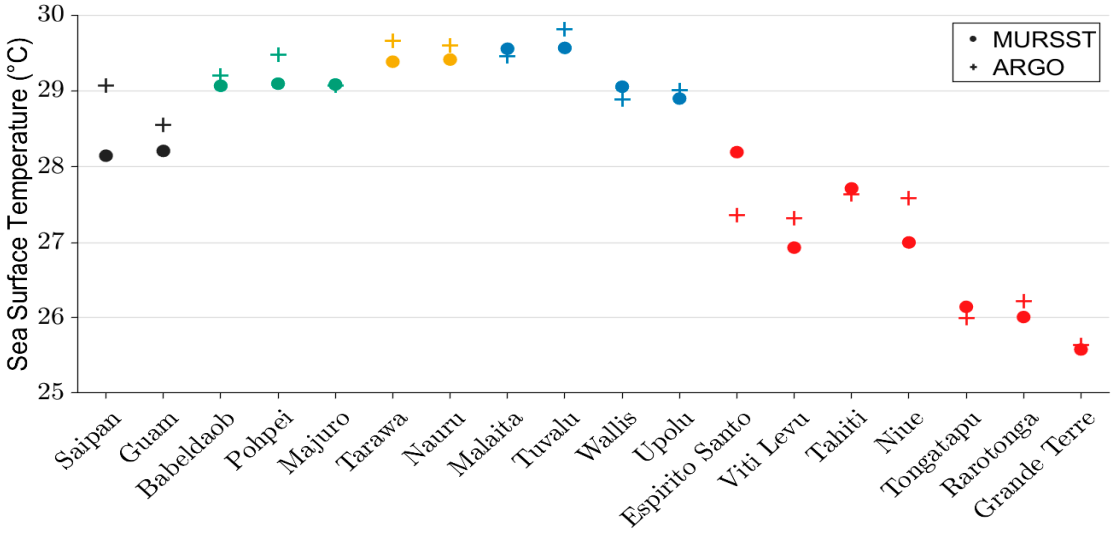


**Figure 12.** SST data comparison between MURSST climatology data and Argo climatology data for the offshore coordinates for each island from Table 3. Comparison was performed using temperature climatology data from 2002 to 2022. Black represents Group 1, green represents Group 2, yellow represents Group 3, blue represents Group 4, and red represents Group 5.

#### 3.3.1. SST Variability

SST climatology data, monthly climatology, and annual means were extracted at the offshore coordinates given in Table 2. To understand the variability of local SST, we presented the minimum, maximum, and standard deviation for monthly and annual means (Table 4). Groups 2, 3, and 4 showed the highest SST climatology as well as the lowest monthly variability, while Group 5, which includes the southernmost islands, showed the highest monthly variability. According to the analysis of the annual mean SST, the highest standard deviation can be found for Groups 3 and 5, including the Equatorial islands of Nauru and Tarawa, as well as the southernmost islands.

**Table 4.** Climatology data for SST (°C), as well as the minimum, maximum, and standard deviation for monthly and interannual climatology data based on the coordinates from Table 2.

| Island | Climatology | Min (Monthly) | Max (Monthly) | Standard Deviation | Min (Annual Mean) | Max (Annual Mean) | Standard Deviation |
|---|---|---|---|---|---|---|---|
| Tuvalu | 29.57 | 28.95 | 30.00 | 0.344 | 29.22 | 29.94 | 0.167 |
| Malaita | 29.56 | 28.94 | 30.00 | 0.351 | 29.23 | 29.93 | 0.165 |
| Nauru | 29.41 | 29.00 | 29.63 | 0.228 | 28.22 | 30.29 | 0.557 |
| Tarawa | 29.38 | 28.92 | 29.65 | 0.251 | 28.20 | 30.23 | 0.543 |
| PohnPei | 29.10 | 28.52 | 29.70 | 0.434 | 28.41 | 29.57 | 0.264 |
| Majuro | 29.08 | 28.51 | 29.70 | 0.433 | 28.41 | 29.57 | 0.264 |
| Babeldaob | 29.07 | 28.48 | 29.70 | 0.441 | 28.39 | 29.55 | 0.272 |
| Wallis | 29.06 | 28.21 | 29.76 | 0.560 | 28.60 | 29.37 | 0.222 |
| Upolu | 28.90 | 28.01 | 29.67 | 0.598 | 28.53 | 29.17 | 0.211 |
| Guam | 28.21 | 27.03 | 29.35 | 0.839 | 27.12 | 28.61 | 0.297 |
| Espirito Santo | 28.19 | 26.90 | 29.43 | 0.950 | 27.30 | 30.62 | 0.602 |
| Saipan | 28.15 | 26.86 | 29.32 | 0.897 | 27.36 | 28.45 | 0.243 |
| Tahiti | 27.72 | 26.49 | 29.02 | 0.895 | 26.96 | 28.20 | 0.295 |
| Niue | 27.00 | 25.59 | 28.56 | 1.085 | 26.08 | 28.20 | 0.406 |
| Viti Levu | 26.94 | 25.28 | 28.70 | 1.276 | 25.81 | 29.23 | 0.621 |
| Tongatapu | 26.14 | 24.45 | 28.03 | 1.297 | 24.81 | 28.10 | 0.592 |
| Rarotonga | 26.01 | 24.31 | 27.94 | 1.322 | 24.67 | 27.95 | 0.592 |
| Grande Terre | 25.58 | 23.51 | 27.84 | 1.584 | 24.27 | 27.73 | 0.615 |

We now investigate the seasonal variations and the interannual variations of the 5 island groups. Figure 13 shows the seasonal variations in the SST, while Figure 14 shows the interannual variability using SST data for the months of October, November, and December to better represent ENSO events. The island of Kumejima has also been included for comparison purposes, as there is an active OTEC experimental plant.

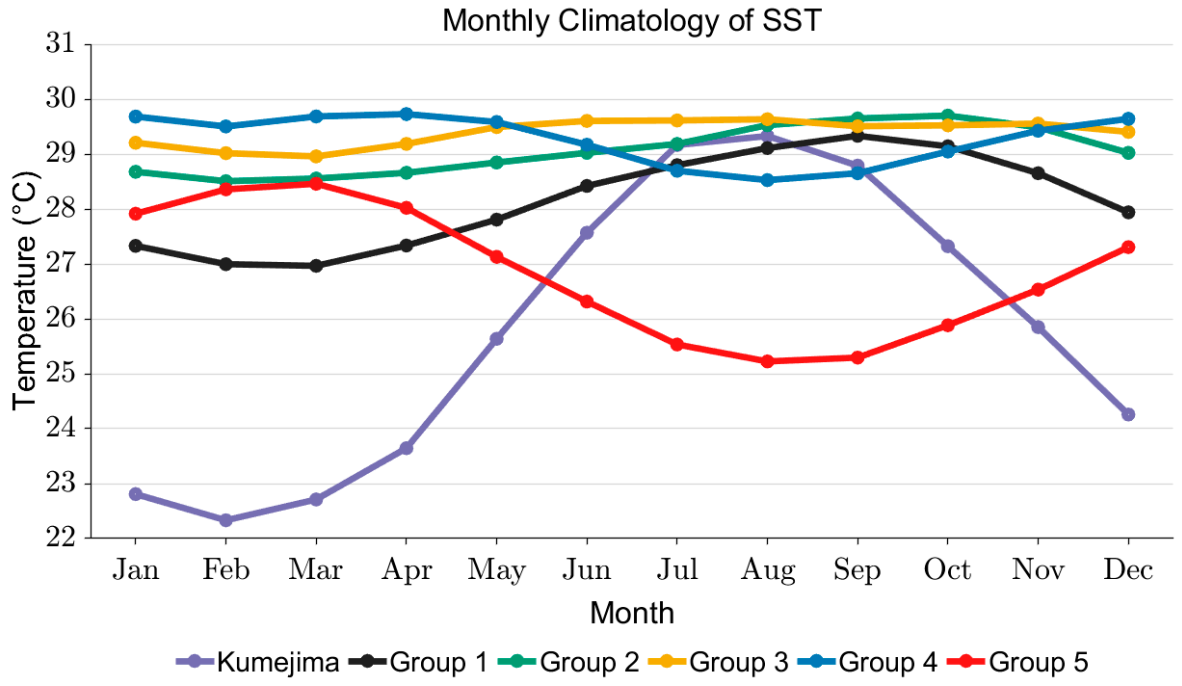


**Figure 13.** Monthly climatology of SST using MURSST data between 2002–2022 for all 18 islands, represented by offshore coordinates from Table 2.

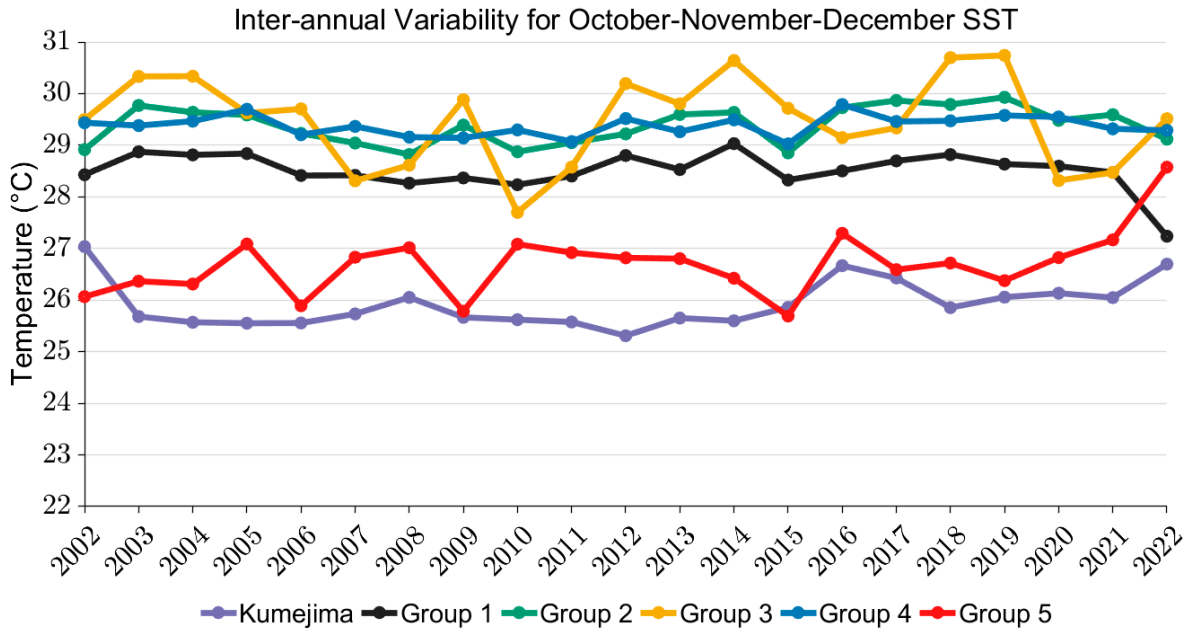


**Figure 14.** Inter-annual variability of SST using yearly averaged data between 2002 and 2022 for all 18 islands, represented by offshore coordinates from Table 2. The averaged temperature values for October, November, and December were selected to better represent ENSO events.

Among all the islands, islands from Group 5, located near the South Pacific, have shown the highest seasonal variability and achieved the lowest SST values from August to September. These islands are located near the Tropics of Capricorn and therefore are most affected by the extra-tropical climate. On the other hand, Groups 3 and 4, which have proximity to the Equator, have the lowest seasonal variability because they are located within the warm pool. They showed that the highest temperatures are from August to October, and the lowest temperatures are from December to March. These features are also visible in Figure 11, where SST seasonal climatology is mapped. We can see that variability for the tropical islands is large, while Equatorial Pacific islands have the least seasonal variability. Overall, the SST variability increases with latitude.

Inter-annual variability follows different patterns for each group (Figure 14). We found that Group 3 had the highest interannual variability among groups, going from its lowest peak at 27.7 °C (2010) to its highest peak at 30.7 °C (2019). This is because Group 3 contains Equatorial Pacific islands, which are prone to SST variability during El Nino and La Nina years. The Oceanic Nino Index (ONI) is plotted in Figure 15, showing the yearly averages of October, November, and December data to identify the effects of ENSO on interannual variability. Group 5 also showed a significant interannual variability from 25.7 °C in 2015 to 27.3 °C in 2016, where large ONI values were also found (Figure 13). This demonstrates that the shift from El Nino to La Nina events in a short period has affected the islands furthest away from the Equator. Interestingly, Groups 1, 2, and 4, which are closer to the Equator in comparison to Group 5, have much lower interannual variability. These comparisons demonstrate the complexity of the SST variations associated with ENSO in the Western Equatorial Pacific. For reference, the SST from the island of Kumejima is plotted in Figures 13 and 14. The SST values from November to May are low compared to the PICTs, monthly variability is high, and the inter-annual variability is significant as the island is in the mid-latitude.

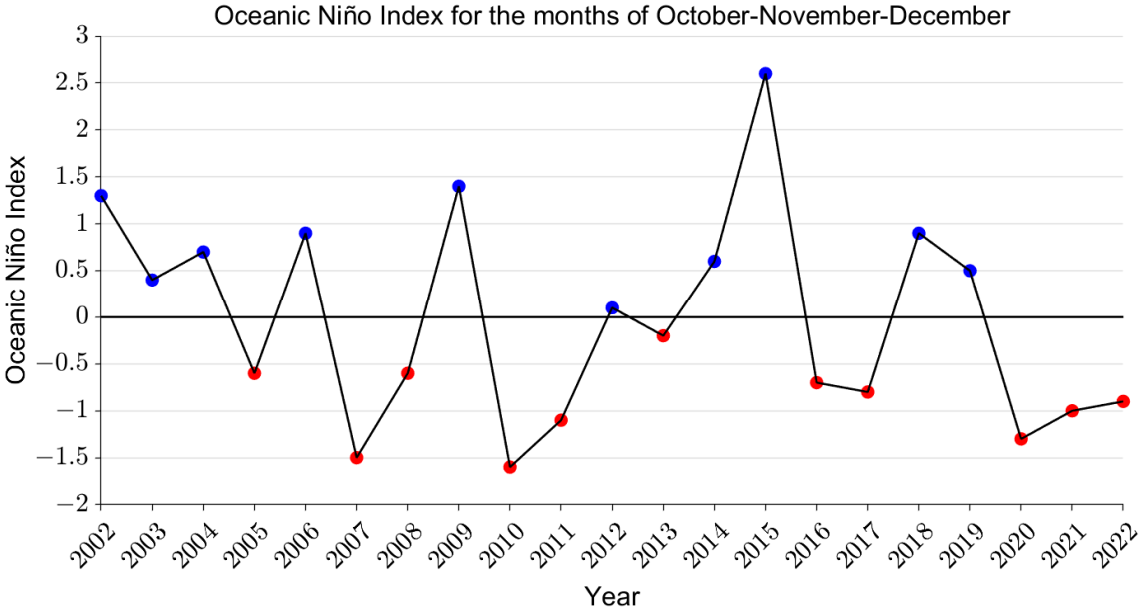


**Figure 15.** Oceanic Nino Index (ONI) for each year from 2002 to 2022 using the average for the months of October, November, and December. Data were taken from NOAA National Weather Service.

To better understand how the ENSO events impact the Pacific Islands, Figure 16 compares the mean SST during 2008, characterized by the La Nina event, and 2015, characterized by the El Nino Event. In 2008 cold SST extended westwards, lowering the temperature at the Equatorial islands, Nauru, and Tarawa (Group 3), and in the Eastern region (no islands). Looking at Figure 16, in the La Nina year (2008), SST decreased from the normal year for Groups 1, 2, and 4, but for Groups 3 and 5, the SST increased.

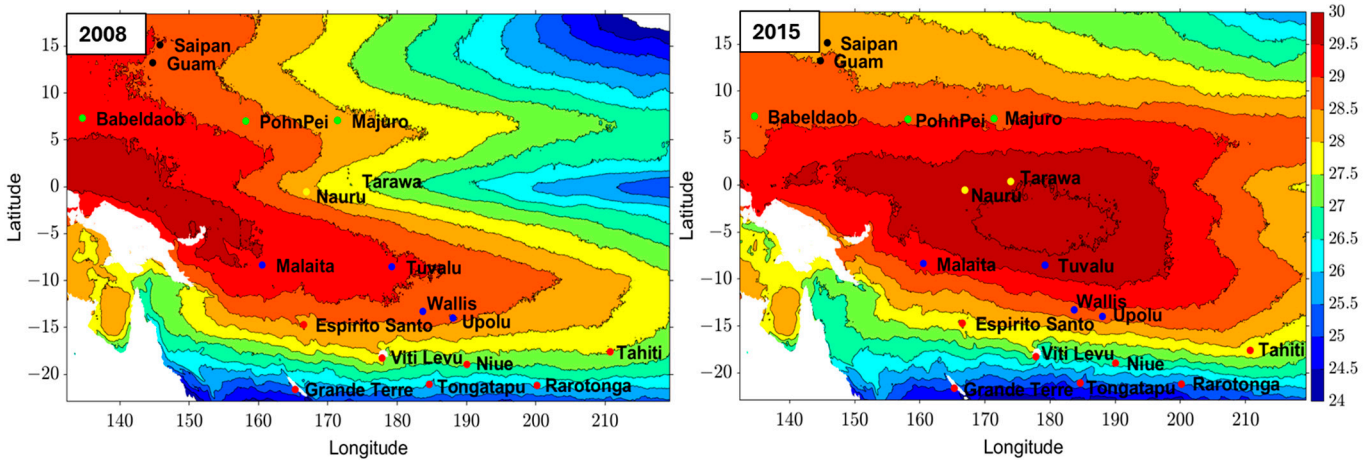


**Figure 16.** Yearly averaged SST data for the years of 2008 (**left**) and 2015 (**right**). The year 2008 was characterized by the La Nina event, while 2015 was characterized by the El Nino event.

During the El Nino year (2015), the center of the Pacific Warm Pool shifted to the east, covering a large area of the Eastern domain of the Western Pacific (the domain given in Figure 16), with temperatures higher than 29 °C. However, none of the 18 islands have shown an increase in SST during this event. Instead, they all showed a negative trend. Group 1, in particular, had the lowest peak temperature during 2015, with an average of 25.7 °C. This is because, in addition to the zonal shift of the warm pool, the meridional extent of the warm pool reduces during the El Nino year. Therefore, all the SST of the 18 islands decreased during the El Nino year. It is important to note that SST increases in the Eastern domain of the Western Pacific, where few inhabited islands exist.

## 4. Resource Assessment of the 18 PICTs

For OTEC analysis, a 700 m depth was chosen to assess ocean thermal resources considering its low standard deviation and the lower costs of the DSW pipes compared to deeper areas (800 to 1000 m).

### *4.1. Ocean Thermal Power Density*

Here, we estimate the ocean thermal power density based on the dead state approximation [18]. If we consider that the equilibrium temperature of the system is $T_0$ (K), heat $Q$ (J) can be estimated as Equation (3), where $T_w$ and $T_c$ are the warm (surface) and cold (deep) water temperature, respectively, $m$ (kg) is the mass, and $c_P$ (J/kg·K) is the specific heat. Here we assumed that heat capacity, density, and volume are the same for both warm and cold systems.

$$Q = mc_P(T_w - T_0) + mc_P(T_0 - T_c) = mc_P(T_w - T_c) \tag{3}$$

The heat density $\overline{Q}$ (J/m$^2$) is given as

$$\frac{Q}{A} = \overline{Q} = (\Delta T)h\rho c_P \tag{4}$$

where $T_W - T_c = \Delta T$, ρ is density (kg/m$^3$), and $m = \rho V = \rho(hA)$. Given the time scale $\Delta s = 1000$ years, which is associated with the deep-water renewal time, the power density $\overline{P}$ (W/m$^2$) is finally derived:

$$\overline{P} = \frac{\overline{Q}}{\Delta s} = \frac{(\Delta T)h\rho c_P}{\Delta s} \tag{5}$$

Here, $h$ represents the height of the water column, typically related to the surface layer where the temperature remains constant. We use a constant value of 100 m based on

previous studies, e.g., the NEDO report for ocean energy potential [19] and the analysis by Nakaoka et al. for the coast of Fiji [20].

First, we estimate the power density in the Pacific domain using HYCOM SST and 700 m depth temperature climatology. Figure 17 shows the $\overline{P}$ (W/m$^2$) climatology for the Pacific domain covering all 18 islands (Table 1). A higher power density was found in the warm pool, where the SST is high. Values throughout the domain vary from 0.257 to 0.322 W/m$^2$, leading to approximately 20% variability that reflects differences in energy production among the islands.

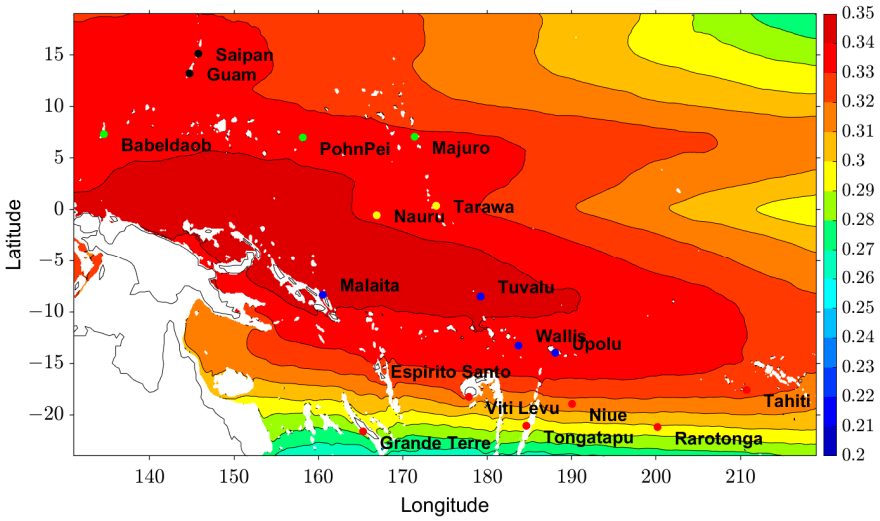


**Figure 17.** Climatology for power density (W/m$^2$) at 700 m depth using HYCOM GOFS 3.1 analysis data (1994–2015) for temperature.

Following the Pacific domain analysis of power density, each island was also individually analyzed using SST climatology from MURSST and the 700 m depth temperature from the averaged Argo temperature profiles. Looking into singular sites on each island allowed us to compare ocean thermal resources among islands. Figure 18 shows the $\overline{P}$ climatology for all 18 islands. Malaita showed the highest $\overline{P}$, at 0.306 W/m$^2$, while Grande Terre showed the lowest $\overline{P}$, at 0.244 W/m$^2$. Even though Tuvalu had the highest values for SST climatology, the DSW temperature at a 700 m depth was lower at Malaita, which led to a higher power density.

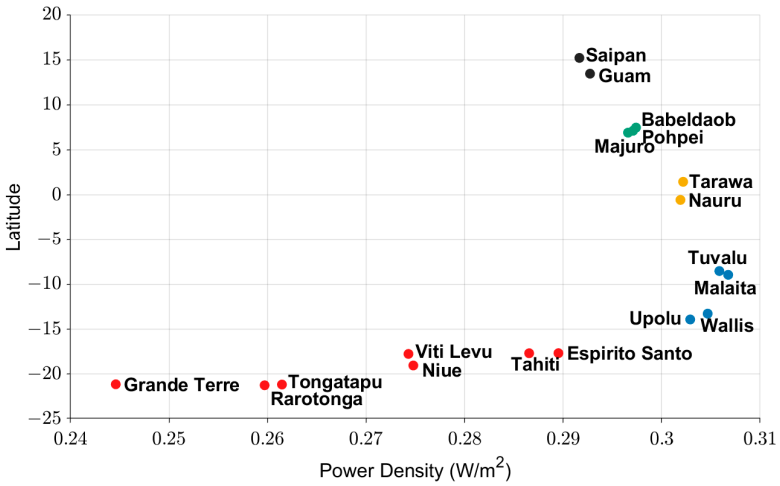


**Figure 18.** Climatology for power density (W/m$^2$) at 700 m versus latitude. Power density was estimated using climatology data for SST and Argo climatology data for 2002–2022 for the offshore coordinates from Table 3.

### *4.2. Design of a 1 MW OTEC System*

The power systems of OTEC can be divided into three categories: closed cycle (CC), open cycle (OC), and hybrid cycle. The main differences between CC and OC are related to the working fluid used for the heat engine, the size of the ducts and turbines, and the heat transfer equipment employed [21]. We give an example of the specification of a CC system following the existing OTEC systems in island environments. Both the Kumejima OTEC Testing facility in Japan [22] and the Makai OTEC plant in Hawaii [23] have demonstrated positive outcomes of combining CC OTEC with DSW industries. Due to the small land size and population size of most selected islands, a small-scale shore-based 1 MW OTEC plant was considered. The OTEC parameters for a 1 MW plant are given in Table 5, where technical parameters were taken from existing literature, e.g., Ref. [24]. OTEC Efficiency was calculated to be around 2% based on the procedure described in the next section.

**Table 5.** Design parameters of the 1 MW OTEC plant considered for analysis.

| OTEC 1 MW Parameters | | |
|---|---|---|
| **Parameter** | **Unit** | **Value** |
| Density ($\rho$) | kg/m$^3$ | 1024.78 |
| SSW Flow Rate ($V_{ww}$) | ton/h | 23,797 [24] |
| | kg/s | 6610.28 |
| DSW Flow Rate ($V_{cw}$) | ton/h | 14,692 [24] |
| | kg/s | 4081.11 |
| In-plant Loss ($P_{Loss}/P_g$) | % | 30 [25] |
| Evaporator Temperature Drop ($\Delta T_E$) | °C | 1.9 |
| Seawater Specific Heat ($c_P$) | J/kg/K | 4000 [25] |
| DSW/SSW Flow Rate Ratio ($r$) | - | 0.62 |
| OTEC Efficiency ($\eta$) | % | 1.99 |
| Annual Operating Hours ($t_A$) | h/year | 7000 [26] |
| Net Power ($P_{net}$) | kW | 1000 |

### *4.3. Net Power and AEP*

Following Nihous (2005) [25], we estimate the gross power ($P_g$) and net power ($P_{net}$) for a standard OTEC process. $P_g$ is the maximum output from an OTEC plant without loss, and $P_{net}$ is the actual power output considering the power loss: $P_{net} = P_g - P_{Loss}$. $P_g$ is defined as a product of thermal power or the input heat transfer of the heat engine ($Q_{in}$) and the thermal efficiency [25]:

$$P_g = \underbrace{Q_{in}}_{\substack{\text{thermal}\\ \text{power}}} \times \underbrace{\eta_{th}}_{\substack{thermal\\ efficiency}} \tag{6}$$

Thermal power is given as $Q_{in} = V_{ww}\rho c_p \Delta T_E$, where the surface water cooling or the temperature drop at the evaporator $\Delta T_E$ is given as

$$\Delta T_E = \underbrace{\left[\frac{r}{(1+r)}\frac{3}{8}\Delta T\right]}_{\substack{\text{surface water}\\ \text{cooling}}} \tag{7}$$

and $r = V_{cw}/V_{ww}$ is the ratio of the cold deep-water flowrate ($V_{cw}$) and the warm surface-water flowrate ($V_{ww}$). Nihous (2005) [25] further assumed an ideal Rankine OTEC power cycle whose efficiency is half of the Carnot cycle. The efficiency is given as

$$\eta_{th} = \underbrace{\left[\frac{\Delta T/2}{T_w}\right]}_{\substack{maximum \\ thermodynamic \\ efficiency}} \cdot \underbrace{\varepsilon_{tg}}_{\substack{turbo \\ generator \\ effciency}} \quad (8)$$

Nihous (2005) [25] found a thermal efficiency of 2.85% based on representative values of the warm and cold water temperature difference $\Delta T = 20$ K and warm water temperature $T_w = 25$ °C or $T_w = 298.15$ K, and $\varepsilon_{tg}$ of 85%.

We estimated OTEC efficiency ($\eta_{th}$) using Equation (8) for all islands (Figure 18). The efficiency varied from 2.66% (Pohnpei) to 3.33% (Babeldaob). Since the efficiency depends on both the warm water temperature $T_w$ (SST) and the temperature difference between surface and deep water $\Delta T$ (SST and 700 m deep water temperature difference), the variation among islands seems larger than the variation in the thermal power density climatology that only depends on $\Delta T$.

The gross power, Equation (6), is the maximum output from an OTEC plant, while there are power losses ($P_{Loss}$) that need to be accounted for [26]. According to Nihous (2005), typical OTEC plant configurations require about 30% of $P_g$ at design conditions, leading to an estimated net power ($P_{net}$) [27,28].

$$P_{net} = P_g - P_{Loss} = P_g - 0.3P_g \quad (9)$$

We can then define the efficiency of the OTEC power plant as a ratio of the work of the heat engine, $W$, to the input heat transfer rate to the heat engine, $Q_{in}$, following Yasunaga et al. (2005) [18]:

$$\eta_{th}{}^{w} = \frac{W}{Q_{in}} \quad (10)$$

Here, the input heat transfer rate is the same as Equation (6), i.e., $Q_{in} = \left(V_{ww}\rho\, c_p\right)\Delta T_E$. If we approximate $W \sim P_{net}$, Equation (8), the mean values of the $\eta_{th}$ of the 18 islands is 3.12%, yielding the mean thermal efficiency based on the work of the heat engine $\eta_{th}{}^{w}$ to be around 2.18% considering a 30% loss.

Yasunaga et al. [24] designed a 1 MW OTEC Plant with a single and double Rankine cycle in Nauru. The design considered the SST and 700 m deep water temperature of Nauru based on a high-resolution ocean model. Based on the design (Table 5), the temperature decreases at the evaporator ($\Delta T_E$) is 1.9 °C, the surface water flowrate $V_{ww}$ is 6.45 $m^3/s$, density $\rho$ is 1024.78 $kg/m^3$, and heat capacity $c_p$ is 4000 J/kg·K. The estimated thermal efficiency $\eta_{th}{}^{w}$ is 1.99%. The estimated value is very close to the mean $\eta_{th}{}^{w}$ of 2.18% based on Equation (8).

Confirming the viability of Nihous' assumption of the 30% loss, we then estimated the Annual Energy Production ($AEP$) (kWh) for the 18 islands, considering a pre-established number of annual operating hours [26] and parameters for the targeted 1 MW OTEC power plant (Table 5):

$$AEP = P_{net} t_A \quad (11)$$

where $t_A$ = 7000 h is the number of annual operating hours, the $P_{net} = 0.7\ P_g$ (kW), and AEP (kWh) is the Annual Energy Production, as shown in Table 6. The target year chosen for AEP estimation was 2022, where the daily SST data were used. The AEP ranges between 7 GWh and 8 GWh and increases from higher latitudes toward the Equator, achieving the highest values at Malaita, followed by Tuvalu, Wallis, and Upolu. All these PICs suffer from energy and water security. For Nauru, the energy demand is around 38 GWh. Therefore, 8 GWh is almost 20% of the total demand. Moreover, according to [18], the desalination plant would require more than 10 GWh per year; thus, having an additional energy supply of 8 GWh per year will be a considerable contribution to the sustainability of the PICs.

**Table 6.** Summary of Annual Energy Production (MWh) in 2022, based on the analysis for all 18 islands (Table 3) using SST climatology and Argo climatology. The temperature difference between SST and 700 m depth water, the SST, and the thermal efficiency $\eta_{th}$ are listed. The 30% loss is applied to all the islands for estimating the AEP.

| Island | ΔT (°C) | SST (°C) | η (%) | AEP (MWh) |
|---|---|---|---|---|
| Malaita | 21.78 | 27.67 | 3.08 | 7574.97 |
| Koror | 23.75 | 29.77 | 3.33 | 8201.82 |
| Tuvalu | 22.78 | 28.76 | 3.21 | 7893.52 |
| Pohnpei | 18.70 | 25.51 | 2.66 | 6549.43 |
| Guam | 23.38 | 29.13 | 3.29 | 8090.39 |
| Saipan | 22.17 | 28.37 | 3.12 | 7692.56 |
| Wallis | 22.99 | 29.33 | 3.23 | 7950.55 |
| Upolu | 23.26 | 29.03 | 3.27 | 8052.00 |
| Majuro | 22.55 | 28.84 | 3.17 | 7811.07 |
| Espirito Santo | 23.34 | 29.59 | 3.28 | 8066.92 |
| Nauru | 23.33 | 29.43 | 3.28 | 8066.10 |
| Tarawa | 22.48 | 28.73 | 3.17 | 7792.02 |
| Tahiti | 21.96 | 27.69 | 3.10 | 7636.32 |
| Viti Levu | 23.22 | 28.88 | 3.27 | 8042.74 |
| Niue | 20.14 | 26.22 | 2.86 | 7039.42 |
| Rarotonga | 20.66 | 26.74 | 2.93 | 7208.38 |
| Tongatapu | 23.31 | 28.99 | 3.28 | 8070.61 |
| Grande Terre | 21.57 | 27.49 | 3.05 | 7506.24 |

Finally, the stability of the AEP is a key factor in lowering the cost of the OTEC plant. In Section 3, we have investigated the interannual variability of SST and the seasonal cycle of SST. The interannual variability of AEP is largest in Group 5, considering the outlier values, particularly Espirito Santo and Viti Levu (Figure 19). The variation reaches almost 1 GWh, which is nearly 15% of the AEP. The variability of these two islands is associated with ENSO, reflecting the interannual variation of the meridional extent of the warm pool (see Section 3.3.1). Likewise, the variabilities of Grande Terre, Tongatapu, and Rarotonga are close to 1 GWh. The reason for this is not evident yet, but considering the complexity of the South Equatorial Current being affected by both ENSO and monsoon, a large variability is expected. Tarawa and Nauru in Group 3 are also affected by ENSO, and their AEP varies around 700 MWh, which is not negligible. Most stable are the islands in Group 4, located upstream of the eastward SECC.

On the other hand, the seasonal variability of the islands in Group 4 is larger than the interannual variability. In Figure 20, we investigate the variability of the monthly climatology of the net power. While the interannual variability was less than 30 kW, the seasonal variability reached around 200 kW. The largest seasonal variability was found in the islands in Group 1 and Group 5, whose latitudes are higher than those of the other groups. Therefore, the seasonality is large. The variation ranges from 400 to 600 kW, which is much larger than the interannual variation of around 100 kW. The seasonal variability is lowest, as expected, near the equator, in Group 3.

Overall, because the seasonal variability is larger than the interannual variability, the total variability of the PICTs seems to be the smallest in Group 3, followed by Groups 2 and 4. These islands have the most stable OTEC resources in the PICTs. However, we should note that the variability in the PICTs is much lower than in Kumejima, where the seasonal cycle of SST was around 7 °C, compared to 2 °C in the PICTs (see Figure 13).

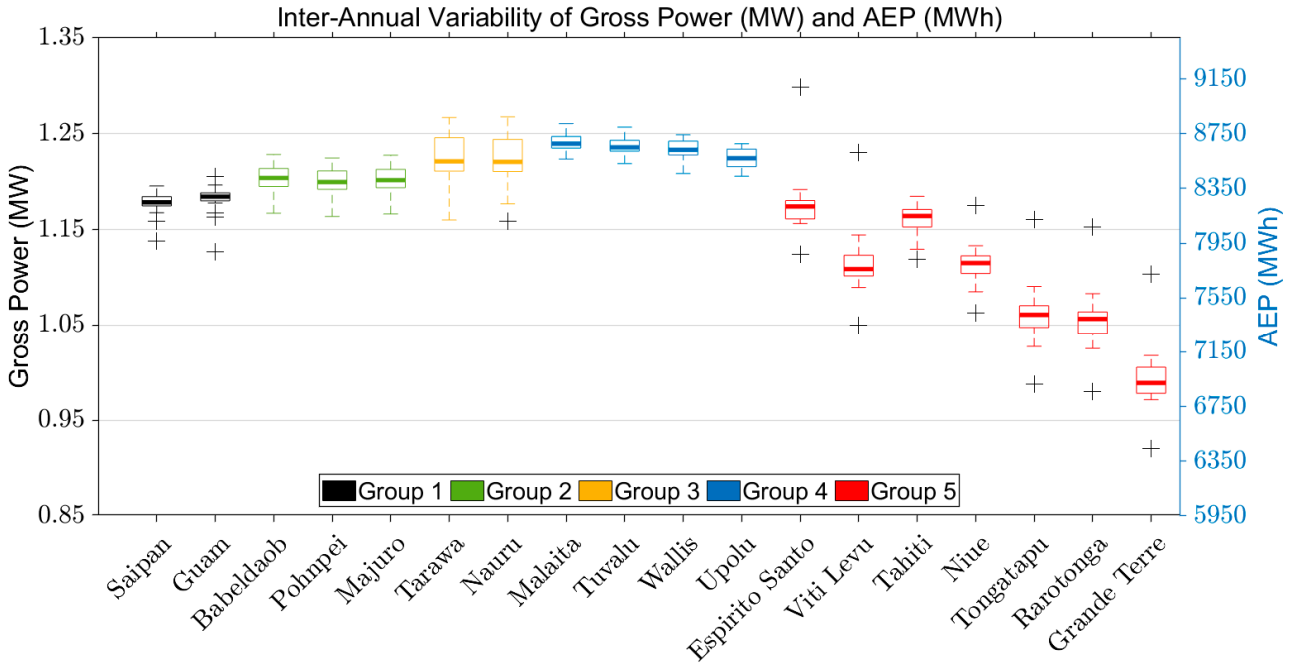


**Figure 19.** Interannual variability of Net Power (kW) and AEP (MWh). The boxes show the median, interquartile range. The outliers of annual mean SST over the 20 years period are shown as "+".

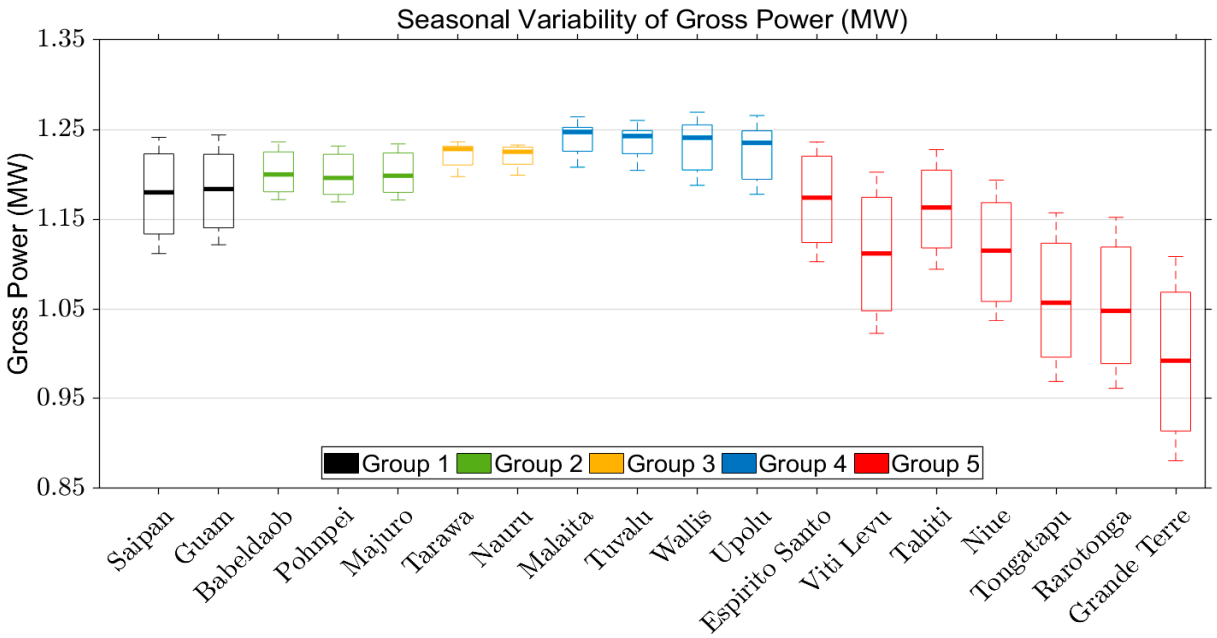


**Figure 20.** The seasonal cycle of Net Power (kW). The boxes show the median, interquartile range, and the outliers of monthly climatology SST over the 20-year period.

## 5. Discussion

Analyzing the newly created 1 km resolution temperature difference data based on satellite data (MURSST) and in situ temperature profile data (Argo), we found differences in ocean thermal energy among the analyzed islands, which are related to their distinct locations and environments. The 18 islands can be divided into 5 main groups that share similarities in terms of SST variability and climatology. The Equatorial islands of Nauru and Tarawa had a distinct temperature profile with small temperature fluctuations below a 400 m depth; as they are located within the EUC, their temperature profiles may indicate strong vertical mixing related to the subsurface current system [29]. Islands in the South

Pacific have shown the lowest values of SST climatology and the highest seasonal variability. Furthermore, islands near the Equator show high values of SST and low seasonal variability. Interannual variability is an important factor that needs to be considered, as the ENSO cycle leads to changes in SST and affects annual energy production.

The development of marine energy projects can be classified into three stages (Figure 21). The first stage is a site screening stage, the second stage is a feasibility study stage, and the third stage is the project design stage. As OTEC projects advance in the PICTs, there is a need for data that can be used at different development stages. In this study, the 20-year-long 1 km dataset combining MURSST and Argo was scrutinized to investigate spatial patterns and seasonal and climate variability within the PICTs. This analysis corresponds to a feasibility study of an OTEC system. The association of the spatio-temporal variability of the temperature field to ocean thermal power has not been attempted before in the Pacific Islands. With these results, we identified groups of islands with similar characteristics and islands with high annual energy production.

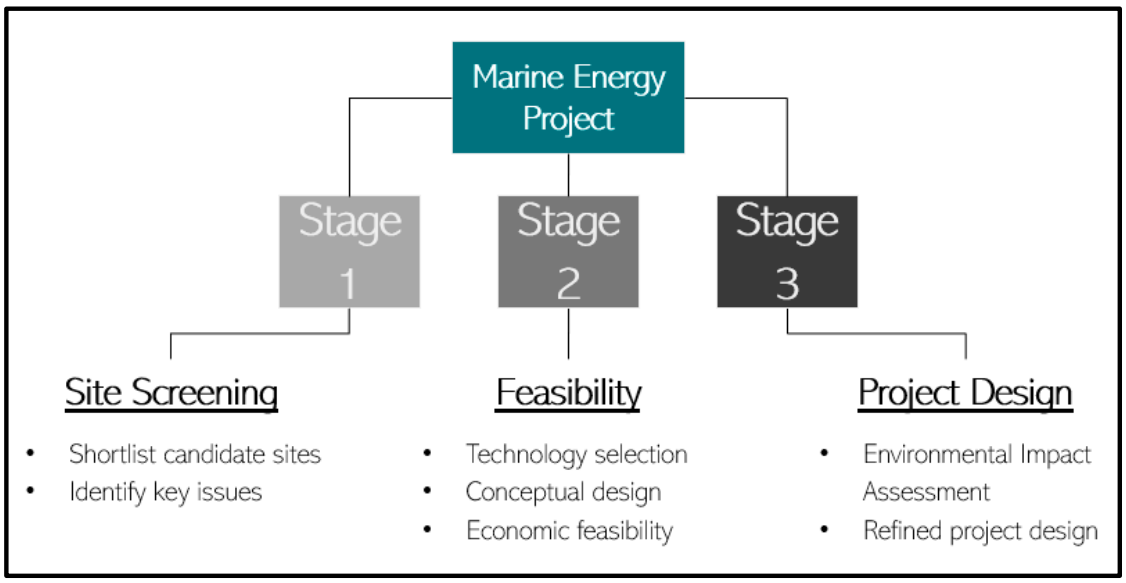


**Figure 21.** Flow chart of Marine Power Project development, showing stages 1 to 3, based on information provided by the European Marine Energy Commission guidelines [30].

HYCOM includes some of the highest-resolution global ocean model data and allows us to estimate global OTEC resources at a 1/12° resolution. HYCOM's reanalysis period is from 2002 to 2015, while the analysis period is from 2015 to now. We compared SST climatology from HYCOM and MURSST during the reanalysis period. Looking at Figure 22, the difference in values remained low in most areas except near the coast and the islands. In the Equatorial region, the SST difference was around 0.2 degrees Celsius. Although the difference is small, amounting to about 2 to 3% in AEP, when temporal change is considered, there may be larger differences caused by transient phenomena such as an island wake.

HYCOM and all the other GOAE products are suitable for site screening (stage 1). Moreover, our analysis demonstrated that having 1 km data for SST was crucial for creating resource maps that can be used for feasibility studies (stage 2). Considering the high computational costs of high-resolution modeling, being able to focus on smaller areas representing suitable sites without conducting high-resolution modeling is a significant advantage to the feasibility assessment process.

However, at the project design phase (Stage 3), even higher-resolution data depending on the local bathymetry and coastline at a few hundred-meter resolution are required. The positive agreement between HYCOM, MURSST, and Argo brings the opportunity to create downscaled models of the PICTs using HYCOM and other GODAE products as boundary

and initial conditions. The high-resolution data can be utilized to design an OTEC plant and to conduct an Environmental Impact Assessment.

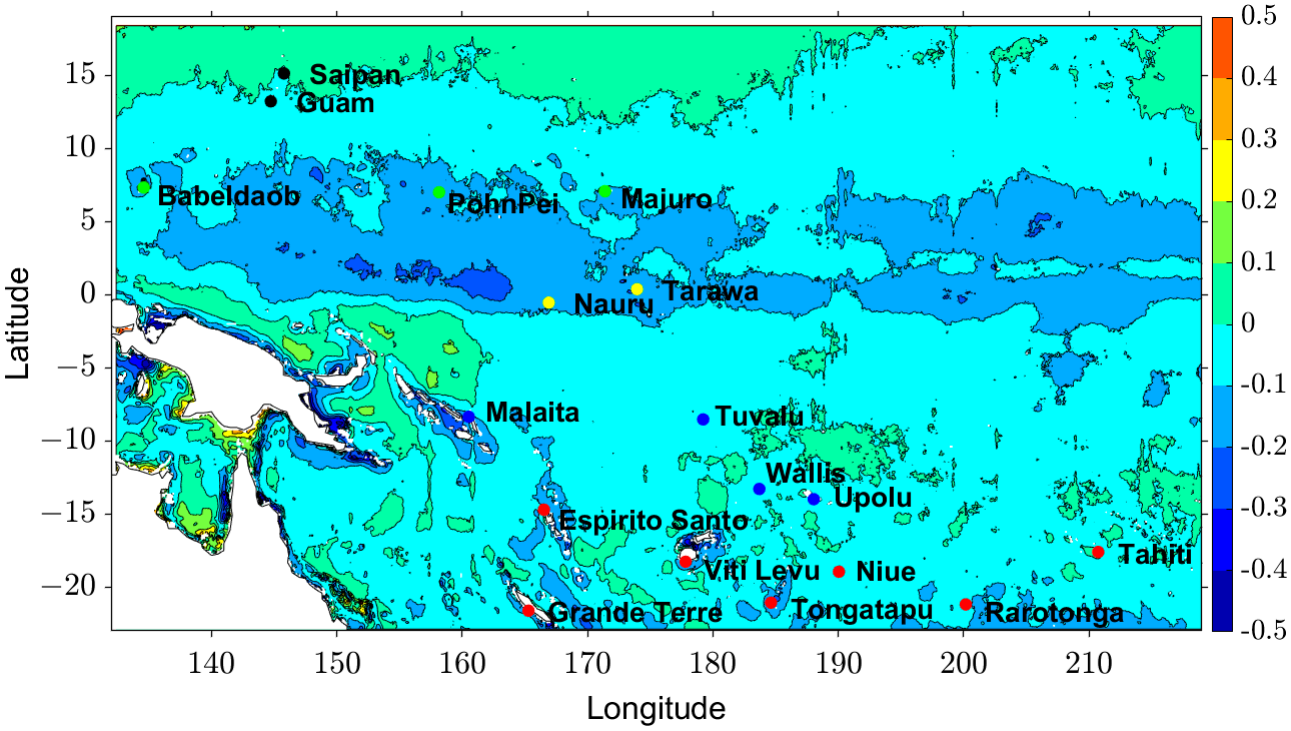


**Figure 22.** Comparison of SST climatology from 2002 to 2015 of MURSST and HYCOM. The island coordinates are offshore coordinates from Table 3. Positive values indicate that HYCOM SST is higher than MURSST.

## 6. Conclusions

The OTEC can not only bring an alternative source of energy to improve energy security but also bring DSW industries that will contribute to different sectors of development within the PICTs. Even though there are datasets available to estimate ocean thermal resources on a global level, high-resolution data are necessary to advance through the stages of a marine energy project. However, the computational cost of creating a downscaled model that includes the 22 PICTs is high. Therefore, a simplified method combining in situ data and high-resolution satellite data was established and applied to the 18 selected islands. The same approach can also be adapted to other locations for OTEC feasibility studies. The output data allowed us to analyze spatial patterns and climate variability of the ocean thermal power within the PICTs. From an oceanographic consideration, we divided the 18 islands into 5 different groups based on the thermocline patterns, the background current fields, and their proximity to the Equator and to the Western Pacific Warm Pool. We successfully analyzed OTEC resources for each group and characterized their seasonal and interannual variability.

As we investigated the 18 sites representing 18 PICTs, we found that there are viable sites in terms of ocean thermal resources. The islands of Malaita, Tuvalu, Pohnpei, Nauru, and Wallis are suitable sites for OTEC, having high power density varying from 0.24 to 0.31 $W/m^2$ and high SST climatology with low seasonal variability. We also tracked the inter-annual variability for each island, revealing the complexity of ENSO effects on the SST among the islands, with more noticeable interannual changes found for Equatorial and southern Pacific islands.

The distance to the shore is another key variable for OTEC development, and among the 18 islands analyzed, we found that 6 islands are located within 1 km of DSW resources. However, if we consider a 2 km distance threshold, the number increases to 14 islands. We suggest conducting further studies to identify potential issues related to OTEC devel-

opment, as additional variables related to the political, economic, social, technological, environmental, and legal sectors might influence the results. Nauru has shown significant advantages—it has high values of SST, high power density, low distance to DSW resources, and low seasonal variability. In this study, we have shown that OTEC has potential in PICTs. OTEC will contribute to different sectors of PICT development as well and add a significant contribution to the Sustainable Development Goals.

**Author Contributions:** Conceptualization, J.B.P.; Methodology, J.B.P. and T.W.; Investigation, J.B.P. and T.W.; Writing—original draft preparation, J.B.P.; Writing—review and editing, T.W.; supervision, T.W., T.Y. and Y.I. All authors have read and agreed to the published version of the manuscript.

**Funding:** A part of this study was funded through the Science and Technology Research Partnership for Sustainable Development (SATREPS) program between Japan and Malaysia, titled "Development of Advanced Hybrid Ocean Thermal Energy Conversion (OTEC) Technology for Low Carbon Society and Sustainable Energy System: First Experimental OTEC Plant of Malaysia".

**Data Availability Statement:** The satellite Sea Surface Temperature data used during this study is available at the National Oceanic and Atmospheric Administration's ERDDAP server (https://coastwatch.pfeg.noaa.gov/erddap/griddap/jplMURSST41mday.html, accessed on 1 February 2024). Temperature profiles were obtained from the data selection tool by the Global Data Assembly Centre (Argo GDAC) (https://dataselection.euro-argo.eu/, accessed on 1 February 2024).

**Acknowledgments:** The authors would like to acknowledge the Science and Technology Research Partnership for Sustainable Development (SATREPS) program and its members, as well as the Institute of Ocean Energy Saga, for supporting this research and providing essential assistance and supervision.

**Conflicts of Interest:** The authors declare no conflicts of interest.

## Appendix A. Argo Cycles

**Table A1.** Number of Argo floats and cycles within the analysis domain from 2002 to 2022.

| Island | Country | N° of Floats | N° of Cycles |
|---|---|---|---|
| Viti Levu | Fiji | 15 | 195 |
| Malaita | Solomon Islands | 30 | 112 |
| Espirito Santo | Vanuatu | 10 | 97 |
| Grande Terre | New Caledonia | 99 | 1545 |
| Tahiti | French Polynesia | 10 | 123 |
| Upolu | Samoa | 6 | 23 |
| Guam | Guam | 6 | 18 |
| Tarawa | Kiribati | 12 | 27 |
| PohnPei | Micronesia | 7 | 17 |
| Tongatapu | Tonga | 5 | 41 |
| Saipan | Northern Mariana | 8 | 18 |
| Majuro | Marshall Islands | 8 | 17 |
| Koror | Palau | 15 | 103 |
| Rarotonga | Cook Islands | 7 | 39 |
| Wallis | Wallis and Futuna | 7 | 18 |
| Tuvalu | Tuvalu | 9 | 29 |
| Nauru | Nauru | 20 | 30 |
| Niue | Niue | 5 | 26 |

## References

1. Dijkstra, H.A.; Neelin, J.D. Ocean-Atmosphere Interaction and the Tropical Climatology. Part II: Why the Pacific Cold Tongue Is in the East. *J. Climate* **1995**, *8*, 1343–1359. [CrossRef]
2. Cummings, J.A. Operational multivariate ocean data assimilation. *Quart. J. Royal Met. Soc. Part C* **2005**, *131*, 3583–3604. [CrossRef]
3. Ocean Thermal Energy Conversion and The Pacific Islands. SOPAC Miscellaneous Report 417, Energy Unit, South Pacific Applied Geoscience Commission Private Mail Bag, GPO, Suva, Fiji Islands. 2001. Available online: https://argonautes.club/images/sampledata/Dossier-energie/pdf/sopacotec.pdf (accessed on 8 October 2020).

4. Luis, V. Economics of Ocean Thermal Energy Conversion (OTEC): An Update. Ocean Energy Recovery—The State of the Art. In Proceedings of the Offshore Technology Conference, Houston, Texas, USA, 3–6 May 2010; Volume 4. [CrossRef]
5. Locarnini, R.A.; Mishonov, A.V.; Antonov, J.I.; Boyer, T.P.; Garcia, H.E. *World Ocean Atlas 2005, Volume 1: Temperature*; Levitus, S., Ed.; NOAA Atlas NESDIS 61, U.S. Government Printing Office: Washington, DC, USA, 2006; p. 182.
6. Kim, H.-J.; Lee, H.-S.; Lim, S.-T.; Petterson, M. The Suitability of the Pacific Islands for Harnessing Ocean Thermal Energy and the Feasibility of OTEC Plants for Onshore or Offshore Processing. *Geosciences* **2021**, *11*, 407. [CrossRef]
7. Petterson, M.G.; Ju Kim, H. *Can Ocean Thermal Energy Conversion and Seawater Utilisation Assist Small Island Developing States? A Case Study of Kiribati, Pacific Islands Region*; IntechOpen: Rijeka, Croatia, 2020. [CrossRef]
8. IRENA. *IRENA—Ocean Thermal Energy Conversion—Technology Brief*; International Renewable Energy Agency: Masdar City, United Arab Emirates, 2014.
9. Asian Development Bank. *Wave Energy Conversion and Ocean Thermal Energy Conversion Potential in Developing Member Countries*; Asian Development Bank: Mandaluyong, Philippines, 2014; Available online: http://hdl.handle.net/11540/51 (accessed on 5 June 2021).
10. Rajagopalan, K.; Nihous, G.C. An Assessment of Global Ocean Thermal Energy Conversion Resources With a High-Resolution Ocean General Circulation Model. *J. Energy Resour. Technol.* **2013**, *135*, 041202. [CrossRef]
11. Bell, M.J.; Schiller, A.; Le Traon, P.Y.; Smith, N.R.; Dombrowsky, E.; Wilmer-Becker, K. An introduction to GODAE OceanView. *J. Oper. Oceanogr.* **2015**, *8* (Suppl. S1), s2–s11. [CrossRef]
12. Powell, B.S. Regional Ocean Modeling System (ROMS): Main Hawaiian Islands. [Indicate Temporal Subset Used] Distributed by the Pacific Islands Ocean Observing System (PacIOOS). 2010, updated 2015. Available online: http://pacioos.org/metadata/roms_hiig.html (accessed on 16 May 2023).
13. Doorga, J.R.S.; Gooroochurn, O.; Motah, B.A.; Ramchandur, V.; Sunassee, S. A novel modelling approach to the identification of optimum sites for the placement of ocean thermal energy conversion (OTEC) power plant: Application to the tropical island climate of Mauritius. *Int. J. Energy Environ. Eng.* **2018**, *9*, 363–382. [CrossRef]
14. Chin, T.M.; Vazquez-Cuervo, J.; Armstrong, E.M. A multi-scale high-resolution analysis of global sea surface temperature. *Remote Sens. Environ.* **2017**, *200*, 154–169. [CrossRef]
15. Rajagopalan, K.; Nihous, G.C. An assessment of global Ocean Thermal Energy Conversion resources under broad geographical constraints. *J. Renew. Sustain. Energy* **2013**, *5*, 063124. [CrossRef]
16. International Hydrographic Organization; Intergovernmental Oceanographic Commission. The IHO-IOC GEBCO Cook Book, IHO Publication B-11, Monaco, 2018; p. 416—IOC Manuals and Guides 63, France, 2018. p. 429. Available online: https://www.star.nesdis.noaa.gov/socd/lsa/GEBCO_Cookbook/documents/CookBook_20191031.pdf (accessed on 16 May 2023).
17. Simpson, J.H.; Sharples, J. *Introduction to the Physical and Biological Oceanography of Shelf Seas*; Cambridge University Press: Cambridge, UK, 2012; p. 28.
18. Yasunaga, T.; Fontaine, K.; Ikegami, Y. Performance Evaluation Concept for Ocean Thermal Energy Conversion toward Standardization and Intelligent Design. *Energies* **2021**, *14*, 2336. [CrossRef]
19. New Energy and Industrial Technology Development Organization. *Research and Development of Wind and Other Natural Energy Technologies/, Research, and Development of Offshore Wind Power Generation Technology/Ocean Energy Resource Assessment*; New Energy and Industrial Technology Development Organization: Washington, DC, USA, 2011.
20. Nakaoka, T.; Nishida, T.; Ichinose, J.; Nagatomo, K.; Mizutani, S.; Tatsumi, S.; Matsushita, M.; Pickering, T.; Ikegami, Y.; Uehara, H. Ocean survey and estimation of energy potential for OTEC in Fiji. *Deep. Ocean. Water Res.* **2003**, *4*, 57–66.
21. Avery, W.H.; Wu, C. *Renewable Energy from the Ocean: A Guide to OTEC*; Oxford University Press: Oxford, UK, 1994.
22. Martin, B.; Okamura, S.; Yasunaga, T.; Ikegami, Y.; Ota, N. OTEC and Advanced Deep Ocean Water Use for Kumejima: An Introduction. In Proceedings of the OCEANS 2022—Chennai, Chennai, India, 21–24 February 2022; pp. 1–5. [CrossRef]
23. McHale, F. Construction and Deployment of an Operational Otec Plant at Kona, Hawaii. In Proceedings of the Offshore Technology Conference, Houston, Texas, 30 April–3 May 1979. [CrossRef]
24. United Nations Industrial Development Organization (UNIDO). Final Report of Ocean Energy Technical Pre-Feasibility Study [Country: Nauru], CTCN Request Reference Number: 2020000016. 2022. Available online: https://www.ctc-n.org/sites/www.ctc-n.org/files/styles/a4_portrait_download/public/pdfpreview/30980-CTCN_Nauru_Pre-Feasibility%20Report_0.png?itok=cFcPGNm3 (accessed on 14 November 2023).
25. Nihous, G.C. An Order-of-Magnitude Estimate of Ocean Thermal Energy Conversion (OTEC) Resources. *ASME J. Energy Resour. Technol.* **2005**, *127*, 328–333. [CrossRef]
26. Basta, G.; Meloni, N.; Poli, F.; Talluri, L.; Manfrida, G. Energy, Exergy and Exergo-Economic Analysis of an OTEC Power Plant Utilizing Kalina Cycle. *Glob. J. Energ. Technol. Res. Updat.* **2021**, *8*, 1–18. Available online: https://www.avantipublishers.com/index.php/gjetru/article/view/1016 (accessed on 5 January 2023). [CrossRef]
27. Nihous, G.C.; Syed, M.A.; Vega, L.A. Design of a Small OTEC Plant for the Production of Electricity and Fresh Water in a Pacific Island. In Proceedings of the ASCE International Conference on Ocean Energy Recovery, Honolulu, HI, USA, 28–30 November 1989; pp. 207–216.
28. Vega, L.A.; Nihous, G.C. Design of a 5 MW Pre-Commercial OTEC Plant. In Proceedings of the Oceanology International, Brighton, UK, 8–11 March 1994; Volume 5, p. 18.

29. Gregg, M.C. Temperature and salinity microstructure in the Pacific equatorial undercurrent. *J. Geophys. Res.* **1976**, *81*, 1180–1196. [CrossRef]
30. Croll, P.; Andina-Pendas, I. *Guidelines for Project Development in the Marine Energy Industry*; Halcrow Group Ltd.: London, UK; European Marine Energy Centre (EMEC): Stromness, UK, 2009.